

# Status and Potential of Lithium Niobate on Insulator (LNOI) for Photonic Integrated Circuits

Andreas Boes,\* Bill Corcoran, Lin Chang, John Bowers, and Arnan Mitchell

Lithium niobate on insulator (LNOI) technology is revolutionizing the lithium niobate industry, enabling higher performance, lower cost and entirely new devices and applications. The availability of LNOI wafers has sparked significant interest in the platform for integrated optical applications, as LNOI offers the attractive material properties of lithium niobate, while also offering the stronger optical confinement and a high optical element integration density that has driven the success of more mature silicon and silicon nitride (SiN) photonics platforms. Due to some similarities between LNOI and SiN, established techniques and standards can readily be adapted to the LNOI platform including a significant array of interface approaches, device designs and also heterogeneous integration techniques for laser sources and photodetectors. In this contribution, we review the latest developments in this platform, examine where further development is necessary to achieve more functionalities in LNOI integrated optical circuits and make a few suggestions of interesting applications that could be realized in this platform.

of the original PIC platforms that enabled optical fiber communications is lithium niobate ( $\text{LiNbO}_3$ ). This can be explained by its material properties, as lithium niobate is robust, has a low-loss transparency window, spanning visible to mid infrared, and has strong electro-optical coefficient ( $r_{33} = 30.8 \times 10^{-12} \text{ m/V}$  at  $\lambda = 0.63 \mu\text{m}$ ).<sup>[11]</sup> Furthermore, lithium niobate has a high second order optical nonlinearity ( $d_{33} = -33 \text{ pm/V}$  at  $\lambda = 1.064 \mu\text{m}$ ) enabling parametric wavelength conversion and optical signal generation,<sup>[12]</sup> making it applicable even during changing standards. However, traditional waveguide fabrication techniques in lithium niobate produce only a subtle index contrast.<sup>[13]</sup> The small index contrast constrains the radius of bending and other adiabatic waveguide structures to the millimeter or even centimeter

## 1. Introduction

In the last decades, research into photonic integrated circuits (PICs) has intensified and PICs are now emerging as a mature and industrial platform, enabling the integration of active and passive optical components on a single chip in a scalable manner. Prominent PIC platforms, which are being developed to industrial scale, are silicon on insulator (SOI),<sup>[1-4]</sup> silicon nitride (SiN),<sup>[5-7]</sup> and indium phosphate (InP)<sup>[8-10]</sup> among others. One

range,<sup>[14]</sup> which limits the ability to integrate multiple optical components on the same chip. This is in stark contrast to the *thin-film* semiconductor platforms, which are currently driving the integrated photonic revolution, enabling increasingly compact and complex integrated systems on a single chip.

Heterogeneous integration of bulk lithium niobate on platforms with a high refractive index contrast enables shorter bending radii and a higher integration density, while the attractive material properties of lithium niobate can still be employed. The heterogeneous integration of lithium niobate with SOI waveguides has attracted significant interest, which enabled electro-optical tunable resonators,<sup>[15-19]</sup> Mach-Zehnder modulators<sup>[20,21]</sup> and Mid-IR modulators.<sup>[22]</sup> Further, multiple die bonding enables integration on 200 mm and 300 mm SOI wafers.<sup>[23,24]</sup> Also SiN, which has nominally a lower refractive index compared to lithium niobate at telecommunication wavelengths, has successfully been heterogeneously integrated with lithium niobate.<sup>[25]</sup> The advantage of heterogeneous integration of SiN and lithium niobate is that both materials are transparent at visible wavelengths, which makes this platform very interesting for future applications in imaging, visualization, sensing and life-sciences. The downside of the heterogeneous integration is that it requires a bonding process, which comes with difficulties such as thermal stress due to different thermal expansion coefficients of the materials and bonding defects due to particles and other impurities.<sup>[26]</sup>


Recently, *thin-film* lithium niobate on insulator (LNOI) has become commercially available. A detailed fabrication process of LNOI wafers and is given by Gorazd Poberaj et al.,<sup>[27]</sup> but for

Dr. A. Boes, Prof. A. Mitchell  
School of Engineering  
RMIT University  
Melbourne, VIC 3001, Australia  
E-mail: andreas.boes@rmit.edu.au

Dr. A. Boes, Dr. B. Corcoran, Prof. A. Mitchell  
ARC Center for Ultra-high Bandwidth Devices for Optical Systems  
(CUDOS)

Dr. B. Corcoran  
Department of Electrical and Computer System Engineering  
Monash University  
Melbourne, VIC 3168, Australia

L. Chang, Prof. J. Bowers  
Department of Electrical and Computer Engineering  
University of California  
Santa Barbara, California 93106, USA

 The ORCID identification number(s) for the author(s) of this article can be found under <https://doi.org/10.1002/lpor.201700256>

DOI: 10.1002/lpor.201700256



**Andreas Boes** is a postdoctoral research fellow in the School of Engineering, RMIT University and a visiting postdoctoral research fellow at the University of California, Santa Barbara. He received his Ph.D. degree from RMIT University in 2015. His research interests include microtechnology, integrated optical circuits, nonlinear optics, optoelectronics and optical communications.



**Bill Corcoran** is a research fellow and lecturer within the Department of Electrical and Computer Systems Engineering at Monash University (Melbourne, Australia). He completed his Ph.D. at the University of Sydney (Sydney, Australia) in 2011 on enhanced optical nonlinearities in silicon waveguides. He held a

postdoctoral research position at Chalmers University of Technology (Gothenburg, Sweden) investigating applications of phase-sensitive optical amplifiers in optical communications systems, before joining Monash in 2013, where he was appointed as an on-going staff member in 2015. His current research topics include topics on optical nonlinearities in fiber optic communication systems, spectral efficiency in optically routed systems, and applications for photonic chips in fiber optic systems.



**Lin Chang** is a graduate student from the University of California, Santa Barbara, where he received his M.S. degree of electrical engineering in 2015. His current research interests are in the field of Silicon Photonics, with an emphasis on nonlinear optics in photonic integrated circuits.



**John E. Bowers** is a Professor in the Department of Electrical and Computer Engineering, University of California Santa Barbara, where he is the Fred Kavli Chair in Nanotechnology and the Director of the Institute for Energy Efficiency. He received the M.S. and Ph.D. degrees from Stan-

ford University, Stanford, CA. He has authored or coauthored eight book chapters, 450 journal papers, and 700 conference papers. He holds 52 patents. Dr. Bowers is a member of the National Academy of Engineering, and a Fellow of IEEE, the Optical Society of America (OSA) and the American Physical Society.

convenience, a brief summary of the process is as follows. LNOI wafers are generally fabricated by a process called “ion-slicing”, which is a similar process used to fabricate industry standard silicon on insulator (SOI) wafers. A high dose of He<sup>+</sup> ions is implanted into a bulk LiNbO<sub>3</sub> wafer. Due to the nature of ion implantation physics, the He<sup>+</sup> ions initially pass through the



**Arnan Mitchell** is a Distinguished Professor in the School of Engineering at RMIT University and Director of RMIT’s Micro Nano Research Facility (MNRF). He received his Ph.D. degree from RMIT University, Melbourne, VIC, Australia. He has authored or co-authored over 400 research

articles. He is a member of the IEEE and the Optical Society of America (OSA). He leads a large multi-disciplinary team with a primary focus on integrated optics, with applications in lab-on-a-chip technologies, microwave photonics and data communications.

LiNbO<sub>3</sub> crystal with little damage until they lose sufficient energy to be able to interact strongly with the crystal. At this point they stop forming an implantation layer where the crystal is significantly damaged and which is rich with He defects. The depth and thickness of this damage layer can be adjusted by controlling the magnitude and spread of the ion acceleration energy. The implanted wafer is then bonded onto another wafer (often also LiNbO<sub>3</sub> but potentially Si or other) that has been coated with a silica buffer layer. This silica buffer layer is bonded to the implanted wafer face and will later act as the insulating layer beneath the LN thin film. The bonding process is performed at elevated temperatures (on the order of 165 to 230 °C),<sup>[27]</sup> which also causes the He in the implantation layer to form gaseous bubbles or blisters, creating a cleavage layer that exfoliates a thin-film of LiNbO<sub>3</sub> onto the silica buffer layer. A final annealing step at 450 to 500 °C is used to further increase the bonding strength of the LiNbO<sub>3</sub> thin-film with the buffer silica layer and recover the LiNbO<sub>3</sub> crystal properties, which may have suffered from the ion implantation process. The final fabrication process of a LNOI wafer is the polishing of the exfoliated LiNbO<sub>3</sub> thin-film to the required thickness with a low surface roughness to reduce scatter losses of optical waveguides.

The standard size of such LNOI wafers is currently three and four inches. Moving to larger LNOI wafer diameters is mainly limited by the availability of larger bulk LiNbO<sub>3</sub> wafers, which are needed for the wafer fabrication process. Wafer sizes up to 125 mm are currently commercially available from companies such as ‘Gooch & Housego’. The “ion slicing” wafer fabrication technology is scalable to larger wafer sizes as the fabrication of SOI wafers with diameter up to 300 mm from companies such as ‘Soitec’ shows. This indicates that the LNOI wafer size can be expected to increase as the fabrication processes mature and the demand increases. The thickness of the lithium niobate thin film, which is bonded on top of the silica buffer layer is usually between 300 and 700 nm. The lithium niobate crystal cut can be freely chosen, although X-cut and Z-cut LNOI wafers are most common. The substrate underneath the silica buffer layer is either lithium niobate or silicon.

Since its market introduction, the LNOI platform has attracted significant interest as it enables the fabrication of ridge and wire waveguides with a significant refractive index contrast, offering many of the advantages enjoyed by other thin-film semiconductor counterparts. Such waveguides possess well confined optical

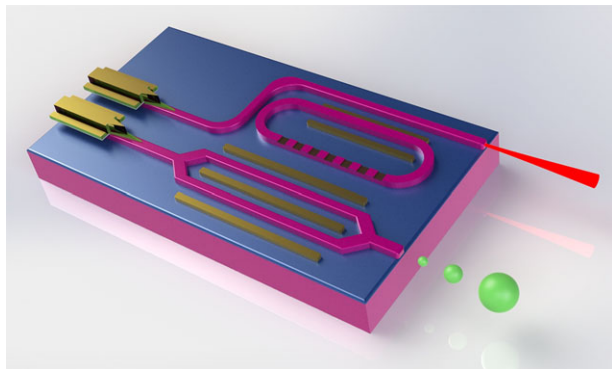


**Figure 1.** Schematically overview of a LNOI integrated optical chip. The bottom photonic integrated circuit illustrates the heterogeneous integration of a laser with an optical intensity modulator in form of a Mach-Zehnder interferometer. The top photonic integrated circuit illustrates the integration of a laser that pumps a nonlinear optical resonator in form of a racetrack for the generation of a frequency comb. The nonlinear optical resonator has a quasi-phase matching section and electrodes for tuning.

modes, resulting in high optical intensities when using moderate optical power, which makes them very attractive for nonlinear optical applications. The buffer silica layer underneath the lithium niobate thin-film improves the electro-optic efficiency of coplanar electrodes on LNOI, by enhancing the overlap of the electrical field with the waveguide mode. The wire or ridge waveguide refractive index contrast also helps to accommodate tighter bending radii on this platform, enabling a high optical component integration density. These properties make LNOI an interesting platform for PICs. Examples of photonic components were reviewed by Gorazd Poberaj et al. in 2012.<sup>[27]</sup>

In this paper, we present an updated review of the current developments in LNOI, identifying optical elements in LNOI that need further optimization and suggesting opportunities where the properties of LNOI PICs can be uniquely valuable. Some examples of new capabilities and new applications are shown in **Figure 1**. It is now possible to integrate lasers and photodetectors and other devices such as isolators and circulators with LNOI devices. Integration improves performance and reliability. For example, integrating the laser pump with the second harmonic generator<sup>[28]</sup> results in better performance because the SHG input coupling losses are removed. The reliability may be better because aging and degradation of the coupling alignment is removed by integration and a pathway is opened to realize systems of electro-optic and SHG components with increasing complexity which would be simply impractical without integration technologies. Indeed, these developments mean that for the first time it is possible to bring the best optical generation, manipulation, routing, detection and nonlinear wavelength conversion onto a single, scalable integration platform.

The paper is structured as follows. Section 2 focuses on the different photonic building blocks that can be combined to achieve highly functional PICs in LNOI. The reviewed building blocks are optical waveguides (2.1), optical interfaces (2.2), electro-optical interfaces (2.3), nonlinear optical elements (2.4), resonant structures (2.5), polarization elements (2.6), gain elements (2.7), and photodetectors (2.8). Section 3 gives some suggestions for LNOI PIC applications in the field of telecommunication (3.1), quan-

tum photonics (3.2) and visible and Mid-IR wavelength photonics (3.3). In the section 4 we summarize the current status of the LNOI platform development for PICs and highlight the remaining challenges and the unique opportunities that can be pursued using this platform.

## 2. Photonic Building Blocks in LNOI

In the following an overview of different photonic building blocks is given. A combination of these building blocks can be assembled to generate highly functional photonic circuits in LNOI. The first and most fundamental building block for PICs in LNOI are optical waveguides, which are reviewed in the next section.

### 2.1. Optical Waveguides

A variety of different optical waveguides have recently been demonstrated in LNOI. For the aim of integrating many optical components on a single chip, one would like to achieve low loss waveguides with a strong optical mode confinement to allow tight waveguide bending radii. In this section, we give a brief overview of the different waveguides in LNOI and discuss their relative merits and trade-offs.

Diffusion based waveguides are well established in bulk lithium niobate, examples are waveguides fabricated by titanium indiffusion or by proton exchange.<sup>[13]</sup> One might think that such diffusion based fabrication methods might also be suitable to laterally confine the optical waveguide mode in LNOI. Titanium indiffusion cannot be used to fabricate waveguides in LNOI as the high annealing temperature ( $\approx 1000$  °C)<sup>[13]</sup> damages the bond between the lithium niobate thin-film and the silica buffer layer, which withstands only temperatures up to  $\approx 500$  °C.<sup>[29]</sup> However, proton exchange takes place at lower temperatures (150–400 °C)<sup>[13]</sup> and was successfully employed to fabricate waveguides in LNOI.<sup>[30–33]</sup> With this fabrication method, waveguide losses down to 0.2 dB/cm for the TE mode<sup>[33]</sup> and 0.6 dB/cm for the TM mode<sup>[31]</sup> have been achieved. However, the refractive index contrast in the in-plane dimension is limited, resulting in a waveguide bending radius in the millimeter length scale.<sup>[33]</sup> The wide waveguide bending radius makes this fabrication technique unsuitable for achieving a high integration density of optical components on PICs. Furthermore, one should keep in mind that proton exchange only increases the extraordinary refractive index, whereas the ordinary refractive index is reduced, which leads to waveguides that only guide light with one polarization.

Wire and ridge waveguides in LNOI are promising as they enable a high integration density and tight waveguide bends due to the stronger refractive index contrast in the in-plane dimension. Removing the lithium niobate around the waveguide core can be used to fabricate wire and ridge waveguides. Several fabrication methods have been demonstrated to achieve the removal of the surrounding lithium niobate. A purely mechanical one has been reported using a precision dicing saw to remove the lithium niobate on either side of the waveguide.<sup>[34–36]</sup> This method achieved waveguides with a loss of 1.2 dB/cm for the TE and 2.8 dB/cm for the TM mode.<sup>[35]</sup> The clear downside of using a dicing saw

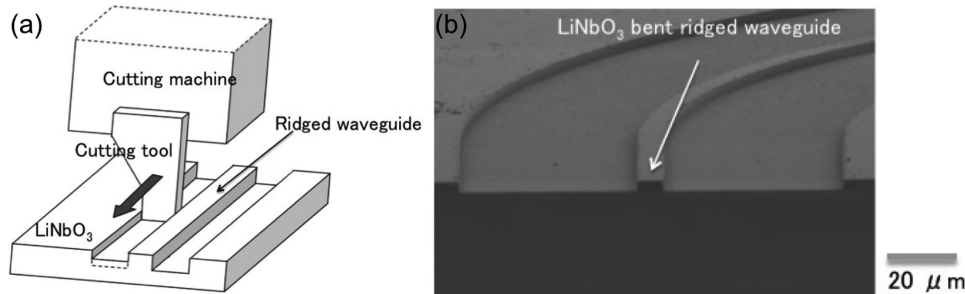


**Figure 2.** a) Illustration of the removal of lithium niobate by using a scraping tool. b) Curved waveguide fabricated by scraping away the lithium niobate on either side of the waveguide. Reproduced with permission.<sup>[37]</sup> Copyright 2014, Optical Society of America.

to fabricate wire waveguides is that only straight cuts and therefore straight waveguides are possible. This makes this fabrication technique unsuitable for achieving more complex PICs on LNOI. A similar purely mechanical method of achieving wire waveguides is the use of an ultra-precision diamond scraping tool as it is illustrated in **Figure 2a**.<sup>[37]</sup> Although this enables curved waveguides (**Figure 2b**), the minimum separation of two waveguides is limited by the width of the diamond tool, which makes small separation between waveguides, (e.g. for waveguide directional couplers into rings), impractical. Furthermore, it has so far only been demonstrated on bulk lithium niobate. On LNOI issues might arise due to the weaker bonding strength of the lithium niobate thin film to the silica buffer layer.

More flexible and high-resolution techniques to remove the lithium niobate on either side of the waveguide core are dry and wet etching. Wet etching has successfully been used to form straight waveguides in bulk lithium niobate<sup>[38]</sup> by using a metal mask and a mixture of hydrofluoric and nitric acid. However, this fabrication approach is limited due to crystallographic dependence of etching rates. This not only reduces the crystal cuts that can be used with this fabrication method, but it may also result in preferential etching along crystal facets, resulting in abrupt changes in sidewall orientation along waveguide bends, which leads to increased scattering losses.

More promising is the fabrication of wire waveguides using dry etching, as it is illustrated in **Figure 3a** to **d**. The first step is to fabricate an etching mask, ideally with a good selectivity compared to lithium niobate, on the LNOI surface (**Figure 3b**). Afterwards the LNOI is etched in a reactive ion etching (RIE) process (**Figure 3c**), followed by the removal of the etching mask (**Figure 3d**), resulting in a wire or ridge waveguide. The dimensions of a single mode wire waveguide for C-band telecommunication wavelengths are usually in the one micron range for the width and a height of 500 to 700  $\mu\text{m}$ . The most critical step of this fabrication sequence is the RIE process. Different gases and parameters have been investigated to dry etch lithium niobate.<sup>[27,39–45]</sup> One of the main issues, when etching lithium niobate with fluoride based gases is the formation of crystalline lithium fluoride (LiF) particles at the surface,<sup>[46,47]</sup> causing a rough lithium niobate surface unsuitable for optical applications. The formation of LiF can be reduced by choosing appropriate etching parameters or exchanging the lithium with hydrogen ions by a proton exchange process.<sup>[39,40,48,49]</sup> The LiF formation can be eliminated by avoiding the use of fluoride based etching gases, such as when using only physical etching by argon milling.<sup>[27,42–45]</sup> This process is

very promising as it was successfully used to achieve wire waveguides with losses as low as 3 dB/cm and bending radii  $<20 \mu\text{m}$ <sup>[50]</sup> for telecommunication C-band wavelengths. The optical losses of the waveguide were further improved by optimizing the waveguide fabrication process, which resulted in an outstanding result with waveguide losses as low as 2.7 dB/m.<sup>[51]</sup> This indicates that this fabrication technique can be used for integrating many optical components on a single PIC.<sup>[50]</sup> A downside of this approach is that the waveguide sidewalls can have a significant angle of  $\approx 40^\circ$  to  $45^\circ$ .<sup>[43,45]</sup> which must be considered in designing the waveguides and can cause issues when fabricating strongly coupled waveguides.

More exotic fabrication techniques for removing the lithium niobate on either side of the waveguide core is the use of focused ion beam (FIB) milling<sup>[52]</sup> or a combination of argon ion irradiation and potassium hydroxide (KOH) etching.<sup>[53]</sup> However, while proof of concept devices have been realized, both techniques are rather slow and cumbersome with FIB milling being a serial process, which cannot easily be scaled to wafer scale production and ion irradiation requiring substantial masking, offering limited control over fine featured geometries.

An attractive alternative to etching the lithium niobate is to form a ridge waveguide by depositing and structuring an optical load material on top of the LNOI as it is illustrated in **Figure 3e** to **h**. The fabrication steps include the deposition of the optical load (**Figure 3e**), followed by the deposition and patterning of the etching mask (**Figure 3f**). Afterwards the optical load material is patterned by an etching process (**Figure 3g**) and the etching mask is removed (**Figure 3h**). Such ridge waveguides are usually wider (approximately 2 to 3  $\mu\text{m}$  wide) compared to the wire waveguides, due to the weaker lateral confinement of the optical mode. Different optical load materials have been tested so far including silicon nitride,<sup>[28,54,55]</sup> titanium dioxide ( $\text{TiO}_2$ ),<sup>[59]</sup> tantalum pentoxide ( $\text{Ta}_2\text{O}_5$ ),<sup>[56]</sup> and chalcogenide glass.<sup>[57]</sup> The most promising optical load material seems to be SiN, as it offers a similar transparency range and refractive index as lithium niobate. Furthermore, SiN is CMOS compatible, which means that the deposition and etching of SiN are standard processes. Low loss SiN can be deposited on the surface of the LNOI by sputtering<sup>[28]</sup> or plasma enhanced chemical vapor deposition (PECVD).<sup>[55]</sup> Using this fabrication approach, waveguide losses as low as  $\approx 0.3 \text{ dB/cm}$ <sup>[28]</sup> and bending radii in the order of 200  $\mu\text{m}$ <sup>[57]</sup> were achieved for telecommunication C-band wavelengths. Lower losses might be achievable by bonding SiN on LNOI, which was deposited by low pressure chemical vapor deposition (LPCVD).<sup>[25]</sup>

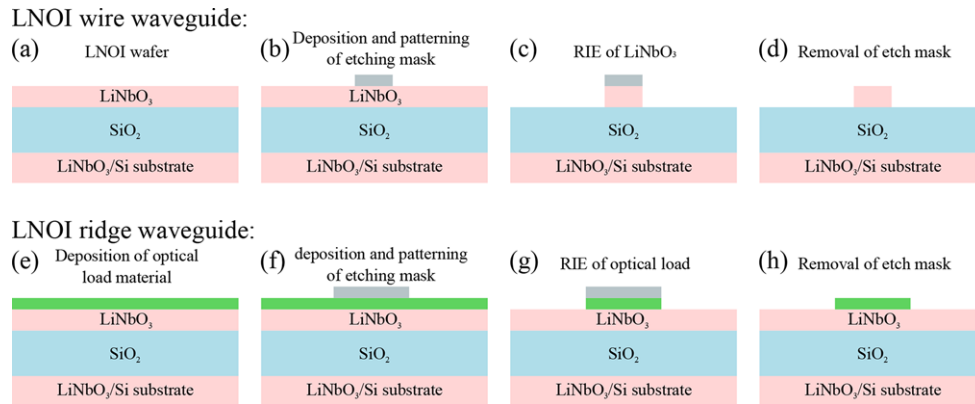


**Figure 3.** The fabrication steps for a wire waveguide by removing the lithium niobate on either side of the waveguide core are illustrated in (a)–(d). A LNOI sample structure is illustrated in (a). b) An etching mask gets deposited and patterned on the LNOI surface, followed by c) a RIE process to remove unprotected lithium niobate. d) The wire waveguide fabrication is completed after the removal of the etching mask. The fabrication steps for ridge waveguide using optical loading are illustrated in (e)–(h). e) First the optical load material is deposited on the LNOI surface. f) Afterwards, an etching mask is deposited and patterned on top of the optical load material. g) The optical load material is then removed on the unprotected areas by RIE, followed by h) the removal of the etch mask to complete the ridge waveguide fabrication.

Wire and ridge waveguides have both their advantages and drawbacks. The smaller interaction area of the optical mode with the sidewall in ridge waveguides results in a lower optical waveguide loss compared to a wire waveguide. The stronger lateral refractive index contrast of wire waveguides enables on the other hand tighter waveguide bending radii, so that a suitable waveguide geometry can be chosen depending on the required waveguide bending radii and optical losses for a specific photonic application. A silica buffer layer on top of the waveguide can help to protect the waveguide and reduce optical losses.

## 2.2. Optical Interfaces

Efficient and easily accessible optical interfaces with photonic circuits on LNOI chip are essential if this platform is to be used practically. In this section, a brief overview of the common coupling methods is given and approaches for applying these coupling methods to wire and ridge waveguides in LNOI are discussed.

Grating couplers are a very attractive method to couple light from a standard optical fiber into and out of waveguides on PICs. The coupling can be done anywhere on the surface of the optical circuit, enabling wafer scale optical testing and the expanded area of most grating couplers provides excellent alignment tolerance. These advantages come at the cost of increased insertion loss and somewhat limited spectral range.<sup>[58,59]</sup> The first grating couplers in LNOI wire waveguides have been demonstrated by etching through a top SiO<sub>2</sub> cladding layer and partially etching into the lithium niobate thin-film.<sup>[60]</sup> The fabricated grating structures and achieved coupling efficiencies can be seen in **Figure 4**. The measured coupling loss per coupler was  $\approx 12$  dB, which is a significant fabrication penalty compared to the simulated coupling loss of  $\approx 4$  dB and shows that the fabrication of the grating couplers needs further optimization. Furthermore, the design of the grating coupler itself can be improved, by adding a bottom reflective layer to increase the coupling efficiency.<sup>[61]</sup>

The potential grating coupler efficiency improvements that are possible can be seen when comparing these results with

grating couplers fabricated in the optical waveguide platform of SiN, which has a similar refractive index compared to lithium niobate, where coupling efficiencies of 4–5 dB per coupler are achievable.<sup>[62–64]</sup> The limited spectra bandwidth and multi dB insertion loss penalty make grating couplers unsuitable for applications where optical power on chip is a priority such as nonlinear optics.

Butt coupling can be used to couple higher optical powers into waveguides with a broad spectral bandwidth. However, butt coupling presents the challenge that there can be a large mode mismatch, in size as well as in shape, between the mode in the optical fiber and the waveguide mode and the small dimensions of the waveguides placing significant demands on alignment tolerances. Increased coupling efficiency has been achieved by using lensed or tapered fibers, with one report demonstrating a loss of  $\approx 6$  dB per facet for the SiN optically loaded waveguides in LNOI.<sup>[28]</sup> Other coupling structures may be needed to improve the butt coupling efficiency even further.

Methods that have been successfully employed to couple light efficiently from standard optical fibers in SOI and SiN waveguides are mode size converters, such as waveguide tapers and inverse tapers. Polymer waveguide tapers have achieved good coupling results on SOI waveguides with coupling loss as low as 0.8 dB/facet.<sup>[65,66]</sup> More complex silicon based tapers were also successfully used to couple light into SOI waveguides with a coupling loss of 2.2 dB/facet.<sup>[67]</sup> Similar schemes and coupling efficiencies should also be achievable for wire waveguides in LNOI, but these have yet to be developed and demonstrated.

Inverse tapers have been successfully implemented in SOI<sup>[68]</sup> and SiN waveguides (see **Figure 5**),<sup>[69]</sup> with coupling losses as low as 0.7 dB/facet. For LNOI waveguides, inverse tapers are suitable for wire waveguides since their mode size can be adiabatically expanded by narrowing the wire waveguide width down. This might be more challenging for optical loaded ridge waveguides, as narrowing down the width of the ridge can result in more of the light residing in the lithium niobate slab creating mode asymmetry.

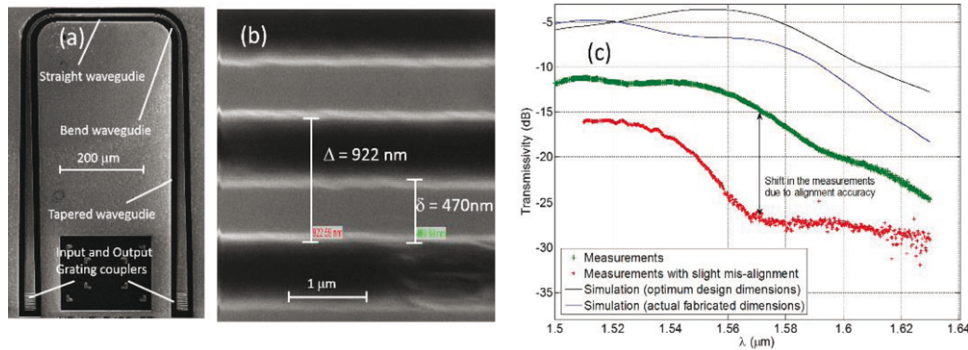


**Figure 4.** a) Grating couplers and waveguide on LNOI. b) SEM image of single grating coupler. c) FDTD simulated (top, blue and black) and experimentally measured (bottom, red and green) transmissivity for a single grating coupler.<sup>[60]</sup> Copyright 2015, Optical Society of America. Reproduced with permission from M. Mahmoud, S. Ghosh, and G. Piazza, CLEO: Science and Innovations, CLEO-SI 2015 (2015).

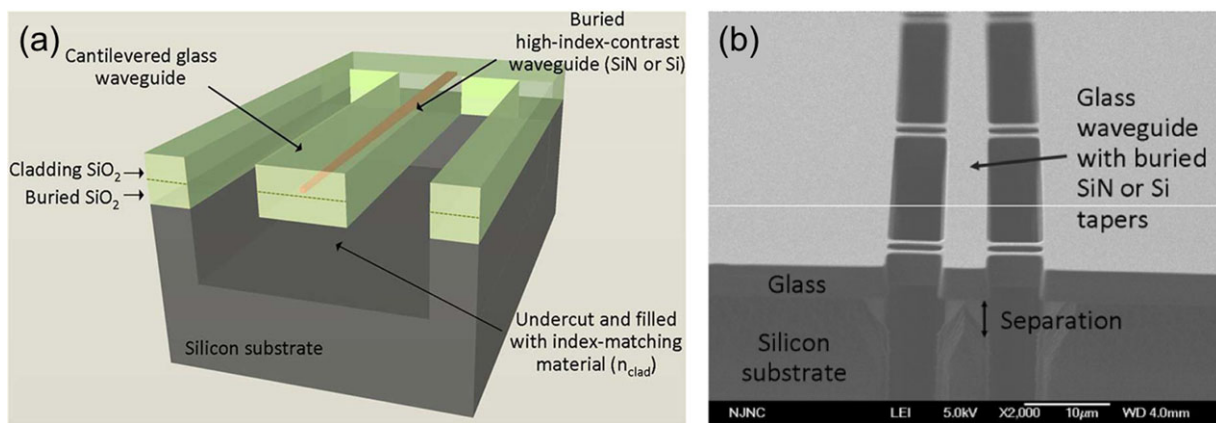


**Figure 5.** a) Schematic of inverted taper to expand the size of the waveguide mode. b) SEM image of the fabricated taper. The coupling losses of the illustrated taper are as low as of 0.7 dB/facet. Reproduced with permission.<sup>[69]</sup> Copyright 2010, IEEE. IEEE Photon. Technol. Lett. **22**, 1744 (2010).

Overall, it can be noted that further investigation and development of optical interfaces is necessary to achieve good coupling efficiencies from standard optical fibers to waveguides on the LNOI platform. However, many advances that have been made on other platforms such as SOI and SiN can be transferred to LNOI waveguides.<sup>[70,71]</sup> One might even consider coupling with high efficiency first to a SiN waveguide,<sup>[69]</sup> which then couples adiabatically to a LNOI waveguide by using appropriate waveguide tapers.<sup>[25]</sup>

### 2.3. Electro-Optical Interfaces

One of the attractive material properties of lithium niobate is the linear electro-optic effect, also known as the Pockels effect, which induces a linear change in refractive index when an electric field is applied to lithium niobate.<sup>[72]</sup> The refractive index change depends thereby not only on the strength of the electric field, but also on the direction of the electric field as it is a tensor product, where the highest electro-optical coefficient in lithium niobate is along the crystallographic Z direction.<sup>[72]</sup>

Changing the refractive index of a lithium niobate waveguides requires the local application of an electric field, which can be achieved by depositing electrodes at the LNOI surface. One can

categorize the use of electrodes on LNOI in two processes that take place at different time regimes, one is the use for ‘slow’ processes such as the tuning of ring resonators in the second to microsecond time range, the other one is for very fast processes such as modulating the optical power using a Mach-Zehnder interferometer in the GHz frequency range.

First, we review the use of the Pockels effect in LNOI for slow tuning processes. Ring resonators and microdisk resonators are widely used in integrated optical circuit designs<sup>[73]</sup> for applications such as filters, nonlinear optical elements and modulators. Ring resonators and microdisk resonators are sensitive to fabrication accuracies and temperature changes, which can shift the resonance frequency response. The resonance frequency shift can be compensated on platforms such as SOI or SiN by heaters that are computer controlled with a feedback loop. However, heaters have a significant energy consumption and are therefore not a very attractive solution for remote applications. Ring resonators and microdisk resonators on LNOI can make use of the electro-optical effect to tune the resonance by applying a semi-static electric field, which consumes less energy. This was successfully done A. Guarino et al.,<sup>[74]</sup> showing that their ring resonator in LNOI (**Figure 6a**) could be tuned by 0.14 GHz/V. Similarly, J. Wang et al.<sup>[75]</sup> showed that a microdisk resonators in LNOI had a tunability of 3.0 GHz/V, shown in Figure 6b.

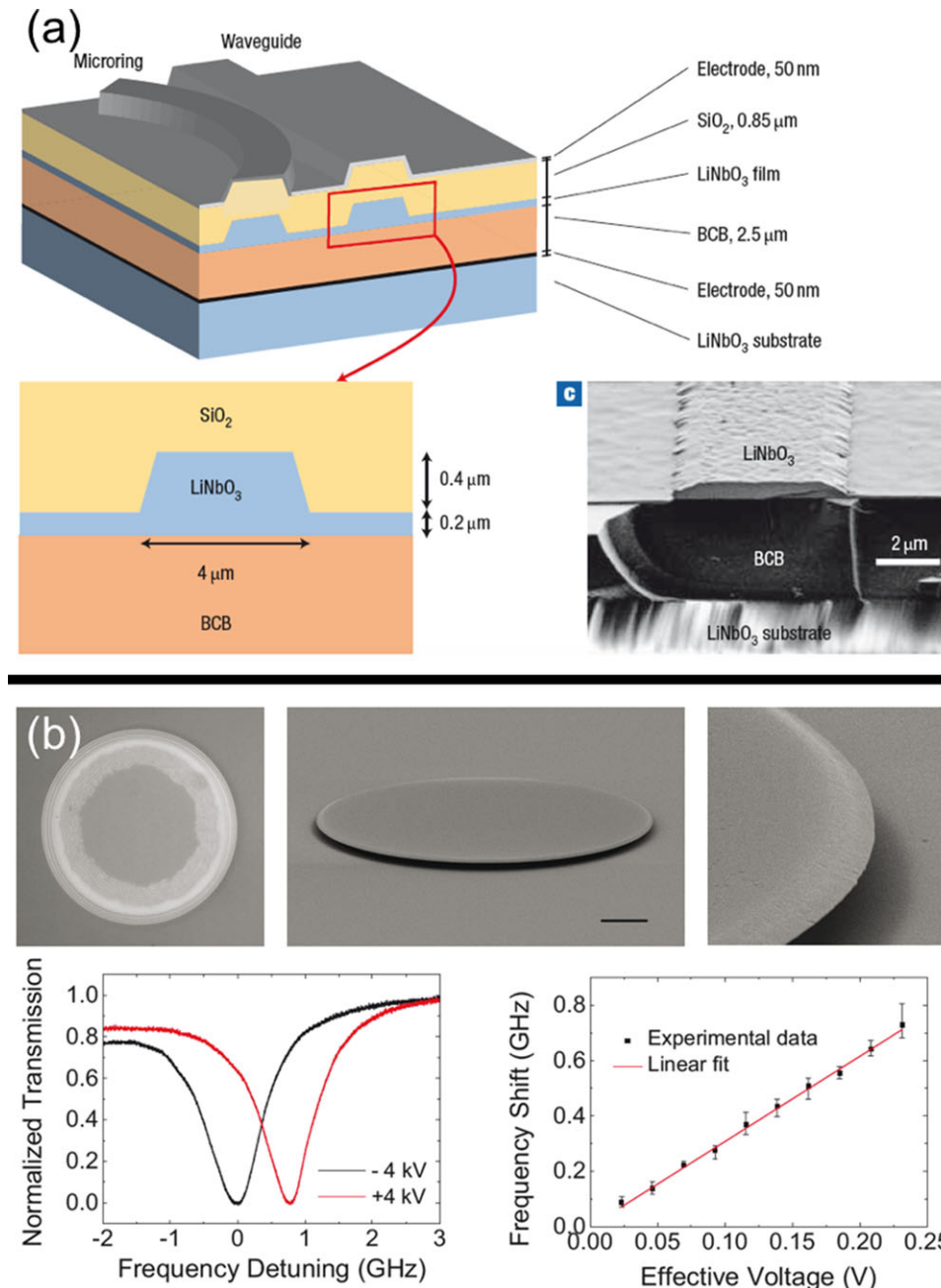


**Figure 6.** a) Electro optical tunable ring resonator by Andrea Guarino et al., achieving a tunability of 0.14 GHz. Reproduced with permission.<sup>[74]</sup> Copyright 2007, Springer Nature. b) Electro optical tunable microdisk resonators by J. Wang et al., achieving a tunability of 3.0 GHz/V. Scale bar in SEM image is 10  $\mu\text{m}$ . Reproduced with permission.<sup>[75]</sup> Copyright 2015, Optical Society of America.

Fast electro optical processes often employ the waveguide structure of a Mach-Zehnder interferometer for modulating the optical power (see **Figure 7b**). Electro-optical modulators in titanium indiffused waveguides are well established and have been used by industry for decades. Transferring the modulation technology to the platform of LNOI is very attractive as the silica layer underneath the lithium niobate thin-film enhances the overlap of the electric field with the optical waveguide mode (as indicated in **Figure 7a**), which increases the modulation

efficiency. This results in a lower electrical power consumption of such modulators, achieving a voltage-length product ( $V_{\pi}L$ ) of 1.8  $\text{Vcm}$ <sup>[50]</sup> and 1.5  $\text{Vcm}$ .<sup>[56]</sup> Further, the lower permeability of the silica layer helps to increase the velocity of the travelling electric wave on the electrodes, so that a lower gold electrode thickness is required in order to match the velocity of the traveling electric wave with the velocity of the optical wave. These advantages have enabled Mach-Zehnder modulators in LNOI that achieve modulating frequencies up to 110 GHz,<sup>[76]</sup> showing that it is a

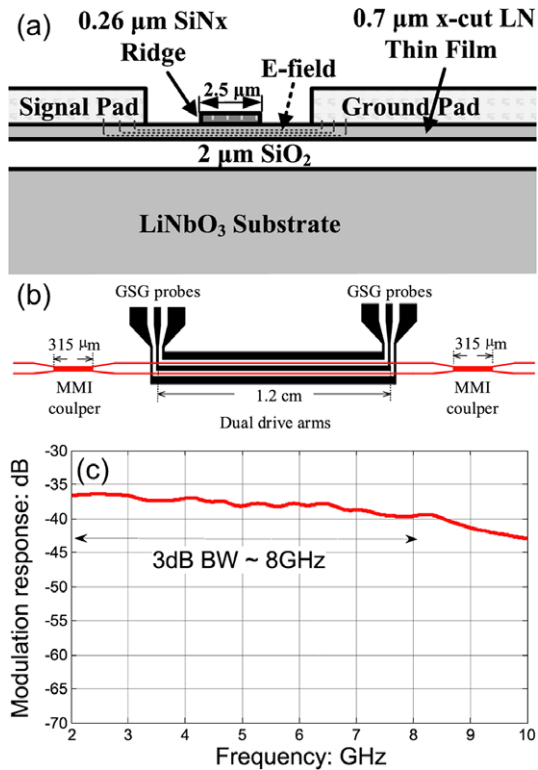


**Figure 7.** a) Illustration of the waveguide cross-section together with the electrodes. b) Schematic of a Mach-Zehnder modulator with multimode interference structures as 3 dB couplers. c) Graph of the modulation response as a function of frequency. Reproduced with permission.<sup>[55]</sup> Copyright 2016, IEEE. IEEE Photon. Technol. Lett. **28**, 736 (2016).

very attractive platform for ultra-fast modulators. Special care needs to be taken for such modulators to achieve an impedance of the electrodes of  $50\ \Omega$ , which reduces unwanted reflections.<sup>[76,77]</sup>

Resonant structures such as ring resonators can also be used for modulating optical signals. The optical intensity modulation is achieved by electro optically shifting the resonator frequency periodically across the laser light frequency, resulting in a periodic low power transmission at the bus waveguide. Wang et al. demonstrated that a resonator in the shape of a ring and a race track can successfully be used for intensity modulation frequencies up to 40 GHz.<sup>[50]</sup> The highest achievable modulation frequency in such resonators is limited by the photon lifetime in the resonator, which depends on the quality (Q) factor of the resonator. This means that a higher Q factor of the resonator will reduce the achievable modulation frequency, whereas a lower Q factor requires higher modulation voltages as the resonant frequency dip is wider.

## 2.4. Nonlinear Optical Elements

Lithium niobate is known to have a high second order nonlinearity, which makes it an interesting material for nonlinear optical processes such as second harmonic generation (SHG), sum and difference frequency generation (SFG and DFG), and spontaneous parametric down conversion (SPDC).<sup>[72]</sup> To achieve

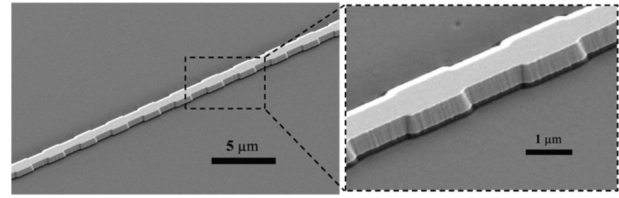


**Figure 8.** Nonlinear optical waveguide in LNOI by spatial modulating the width of the waveguide with a period of  $2.77\ \mu\text{m}$  and a groove depth of  $80\ \text{nm}$ . Reproduced with permission.<sup>[45]</sup> Copyright 2017, Optical Society of America.

efficient frequency conversion in lithium niobate, the phase velocity of the interacting wavelengths either have to be the same or alternatively have to be compensated by schemes such as quasi-phase matching (QPM)<sup>[78]</sup> or modal dispersion phase matching (MDPM). MDPM has recently been used in LNOI proton exchange and wire waveguides, achieving SHG with a conversion efficiency of  $48\% \text{ W}^{-1}\text{cm}^{-2}$  and  $41\% \text{ W}^{-1}\text{cm}^{-2}$ , respectively.<sup>[30,45]</sup> The phase matching condition was fulfilled by carefully designing the waveguide properties to phase match the fundamental mode in the infrared wavelength regime with a higher order SHG mode.

Wang et al.<sup>[45]</sup> showed that one can also achieve a nonlinear optical element in LNOI by periodically altering the wire waveguide dimensions, as it is shown in Figure 8. By doing so, an additional momentum difference  $\Delta k = 2\pi/\Lambda$  could be applied to the propagating electromagnetic wave, compensating for the phase mismatch, which resulted in a conversion efficiency of  $6.8\% \text{ W}^{-1}\text{cm}^{-2}$  of the fabricated waveguide.

In LNOI waveguides, QPM can be achieved by inverting the spontaneous polarization of the lithium niobate crystal periodically along the waveguide. The inversion of the crystal direction, also called domain inversion, can either be done before the lithium niobate thin-film is bonded on the silica buffer layer<sup>[79]</sup> in the LNOI wafer fabrication process or afterwards on the LNOI wafer itself.<sup>[28,54,80,81]</sup> A method to generate domain patterns on LNOI is the electric field poling technique. This technique reverses the direction of the spontaneous polarization by locally applying an electric field along the polar z-axis of the crystal, exceeding the so-called coercive field.<sup>[82]</sup> On LNOI wafers the geometry and position of the electrodes depends on the crystal cut that is used. For a Z-cut LNOI wafer the electrodes for applying the electric field should be above and below the lithium niobate thin-film. This has been achieved by using a conductive atom force microscope (AFM) tip on the top surface and a ground electrode underneath the lithium niobate thin film (Figure 9a). The crystal's spontaneous polarization can be locally inverted by applying a voltage to the AFM tip, which exceeds the coercive field.<sup>[81]</sup> This domain engineering method offers the possibility to directly write domain patterns in LNOI and achieve a very high resolution with domain sizes smaller than  $100\ \text{nm}$ . The drawback of this domain engineering method is that it is a serial process and therefore rather slow. Furthermore, the domain inversion process requires a conductive ground electrode underneath the lithium niobate thin film, which may limit its use for optical waveguide applications. The literature is currently not conclusive on the stability of the inverted domains when an AFM is used. Gainutdinov et al.<sup>[81]</sup> indicated that the AFM written



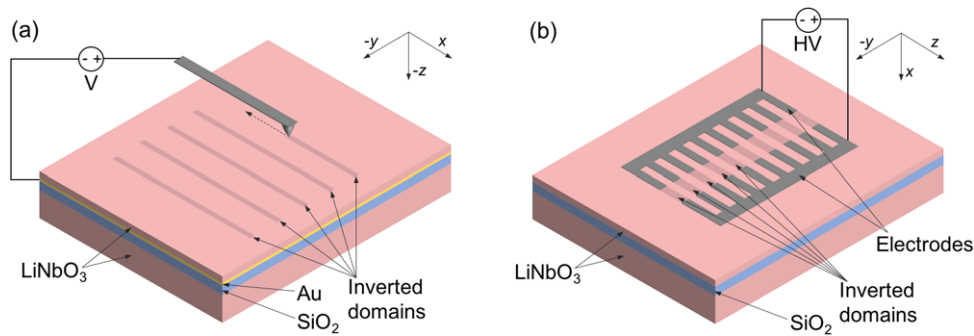


**Figure 9.** a) Periodic domain engineering for QPM structures in Z-cut LNOI can be achieved by applying a voltage to a conductive AFM tip and scanning it across the surface of a LNOI sample, where the ground electrode is between the lithium niobate thin film and the silica layer. b) A method to achieve QPM structures in X-cut LNOI is by patterning metal electrodes on the surface and applying a strong electric field to them, causing domain inversion. The period of the QPM pattern is defined by the finger period.

domains are stable, whereas Shao et al.<sup>[83]</sup> found that the inverted domain life time is in the order of 25 h for a 540 nm thick lithium niobate thin-film. Therefore, the domain stability of AFM written domains has to be further investigated.

For X-cut LNOI wafers, two digitated electrodes can be patterned on the surface of the LNOI wafer to generate a periodic poling pattern, where the poling period is determined by the finger period. The electrode fingers are oriented along the crystallographic Z-direction as it is illustrated in Figure 9b. The domain inversion process occurs when a high voltage is applied to one electrode and the other electrode of the pair is connected to ground, which generates a high electric field at the tips of the electrode fingers exceeding the coercive field.<sup>[80]</sup> The fingers separation is in the order of tens of microns and the applied voltages are in the order of several hundreds to a few thousand volts. This domain engineering method has successfully been used to achieve domain inversion with periods down to 2.4  $\mu\text{m}$ .<sup>[28]</sup> The literature indicates that the inverted domains with this method are stable.

The periodic domain patterns achieved using digitated electrodes on X-cut LNOI wafers have successfully been used for nonlinear optical applications,<sup>[28,54]</sup> in ridge waveguides fabricated by SiN optical loading (Figure 10a). Conversion efficiency of up to 160%  $\text{W}^{-1}\text{cm}^{-2}$  have been achieved as indicated in Figure 10c. This domain engineering method is therefore a very promising fabrication method for achieving highly efficient nonlinear optical elements in LNOI. However, simulations predict that conversion efficiency of up to 1600%  $\text{W}^{-1}\text{cm}^{-2}$  should be achievable in these waveguides, which is one order of magnitude higher than the ones experimentally observed.<sup>[28]</sup> This indicates that further investigations are necessary to achieve the predicted nonlinear optical efficiencies in such waveguides.

Resonant structures can also be used as nonlinear optical elements in PICs and will be discussed in more detail in the next section.

## 2.5. Resonant Structures

Resonant structures find a variety of uses in PICs such as wavelength filters, nonlinear optical elements and sensors. In this sec-

tion we discuss resonant structures, such as microdisks, ring resonators, and photonic crystals that have been realized in LNOI.

Microdisk resonators or whispering gallery mode (WGM) micro resonators confine light at the edge of the resonator via total internal reflection, which can lead to remarkably high optical intensities. The microdisks are fabricated by patterning the thin-film lithium niobate in a circular disk shape. The silica layer underneath the disk is partially removed by hydrofluoric etching, only leaving a silica pedestal in the disk center behind. An example of a typical microdisk resonator is shown in Figure 11. Such microdisks have been investigated for nonlinear optical,<sup>[84]</sup> electro-optical,<sup>[85–89]</sup> and optomechanical applications.<sup>[90,91]</sup> The Q factors achieved in such LNOI microdisks are in the order of  $10^5$  to  $10^6$  with disk radii ranging from 6 to 40  $\mu\text{m}$ .<sup>[85–90]</sup>

Ring resonators are very similar to microdisks, with the difference that ring resonators have usually a single mode waveguide as a guiding structure. Ring resonators have been fabricated in LNOI by a number of researchers. Siew et al.<sup>[43]</sup> fabricated a ring resonator with a bending radius of 50  $\mu\text{m}$  and a Q factor of  $\approx 2,800$ . Similarly, Guarino et al.<sup>[74]</sup> fabricated a ring resonator with a bending radius of 100  $\mu\text{m}$  and a Q factor of  $\approx 4,000$  using ridge waveguides. Wang et al.<sup>[50]</sup> fabricated resonators in shape of a ring and a race track, and achieved Q factors up to  $\approx 50,000$ . However, one should note that the focus of Wang et al. was not to achieve very high Q factors, as they used the ring resonators to modulate light.<sup>[50]</sup> The same group demonstrated shortly afterwards exceptional Q factors up to  $10^7$  in LNOI waveguides using an optimized design and waveguide fabrication technique.<sup>[51]</sup>

Photonic crystals are periodic dielectric structures, which forbid the propagation of certain wavelengths of light due to the existence of a band gap.<sup>[92]</sup> The dielectric periodicity is usually achieved by removing the optical guiding material periodically, for example by drilling holes using focused ion beam milling (FIB). Such photonic crystals are attractive as they offer the possibility of ultra-small and efficient filter and nonlinear optical devices. An example is a one dimensional photonic crystal with a defect (Figure 12), which has been fabricated in a LNOI optical waveguide, showing that such a structure has a band pass filter spectral characteristic.<sup>[52]</sup> The extinction ratio of this filter was 12.5 dB and the cavity had a Q factor of 156. Recently, a

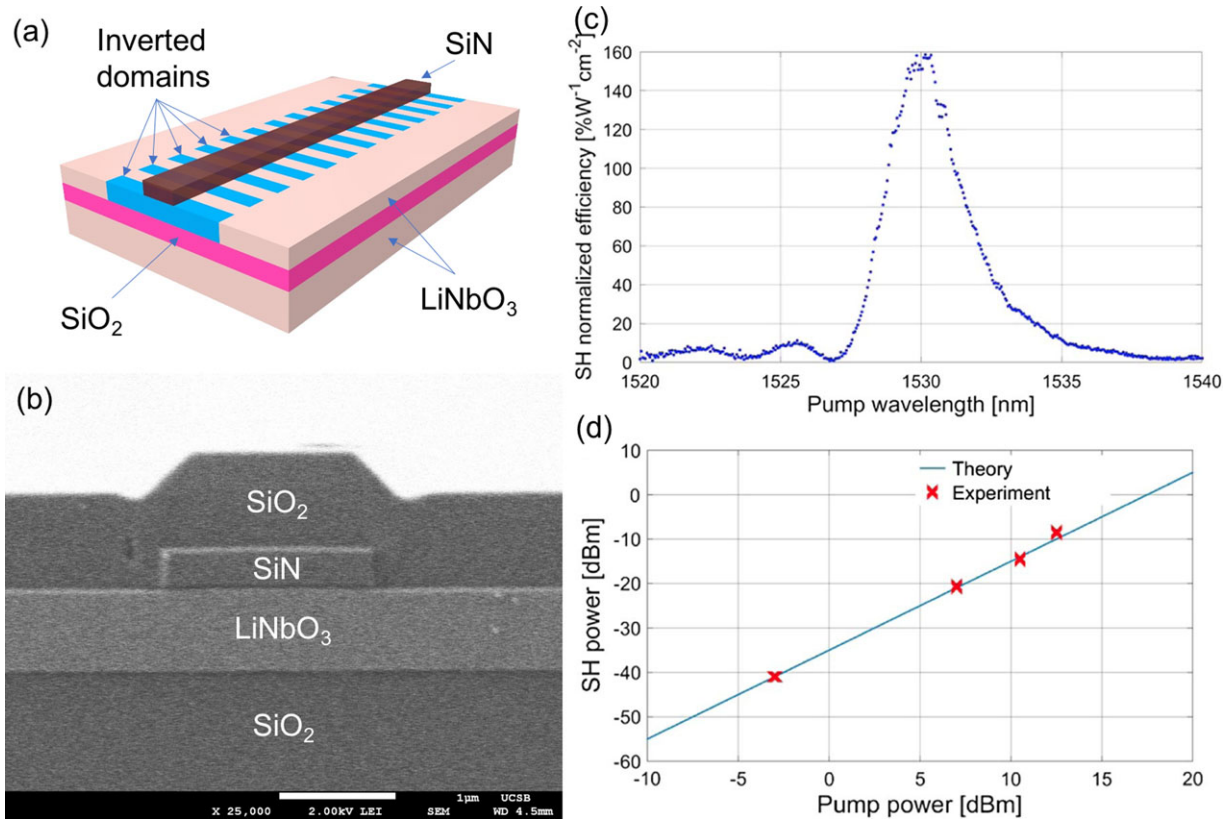


**Figure 10.** a) Schematic of a periodically poled LNOI waveguide with SiN as optical loading material. b) Cross-section of a SiN optically loaded waveguide. c) Normalized efficiency as a function of the pump wavelength for a periodically poled ridge waveguide in LNOI, which was fabricated by patterned SiN loading. d) Peak generated SH power under different pump powers (red crosses). Reproduced with permission.<sup>[28]</sup> Copyright 2016, Optical Society of America.

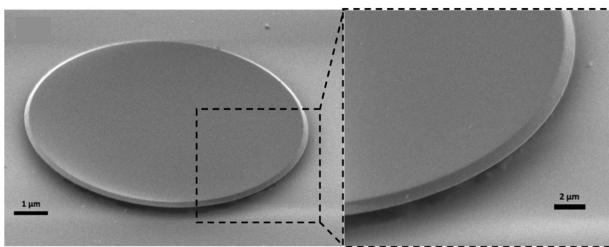


**Figure 11.** SEM image of a suspended 400 nm thick and 28 μm diameter lithium niobate microdisk supported by a silica pedestal on top of a LN substrate. Reproduced with permission.<sup>[85]</sup> Copyright 2014, Optical Society of America.

photonic crystal nanobeam resonators with optical  $Q$  as high as  $10^5$  has been demonstrated in LNOI.<sup>[93]</sup> This is an outstanding achievement, as the  $Q$  is two orders of magnitude higher compared to previous results. The high optical  $Q$ , together with tight optical mode confinement, lead to a cavity resonance tuning of  $\approx 0.64$  GHz/aJ, corresponding to  $\approx 84$  MHz/photon, which is caused by the photorefractive effect. Two dimensional photonic crystals have also been fabricated in LNOI and their band structure at C-band telecommunication wavelengths studied.<sup>[94]</sup> The inclusion of a defect in a two dimensional photonic crystal can

be used to form a cavity and the nonlinear optical properties of such a cavity has been investigated when it was used for SHG.<sup>[95]</sup> The  $Q$  factor of the cavity for the fundamental wavelength was 678. This shows that photonic crystals are interesting options to form a building block in LNOI photonic circuits.

The fabrication of Bragg gratings in bulk lithium niobate is well established, as they can be fabricated in iron or copper doped lithium niobate using holographic illumination techniques.<sup>[96]</sup> The fabrication of Bragg grating by removal or etching of lithium niobate has also been investigated,<sup>[97,98]</sup> however in weakly guided waveguides such techniques can suffer from significant scattering loss due to the weak confinement. For LNOI waveguides this is less of an issue due to the higher refractive index contrast of the optical waveguide, so that Bragg grating similar to what has been established in SiN waveguides<sup>[99]</sup> can potentially be realized on LNOI.

## 2.6. Polarization Elements

The optical properties of lithium niobate depend strongly on the polarization of the optical wave. This strong dependence can be explained by lithium niobate's natural birefringence and by the fact that the nonlinear optical and electro optical coefficients

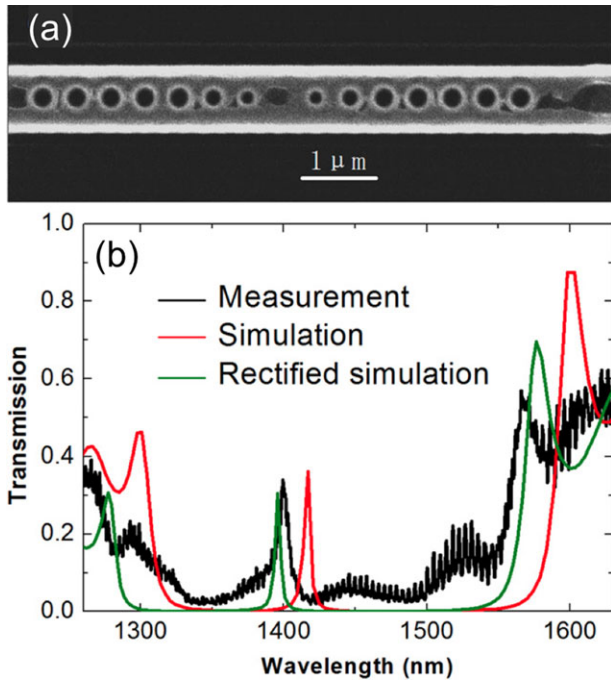


**Figure 12.** a) Photonic crystal micro-cavity with lattice constant  $a = 450$  nm, radius of holes  $R = 0.25a$ , and two holes with radii of 0.8 and 0.6R on each side of the cavity. Measured (black line) and simulated (red line) normalized transmission of the PC micro-cavity. Reproduced with permission.<sup>[52]</sup> Copyright 2016, Institute of Physics and IOP Publishing.

are tensors. This shows that optical elements that can control the polarization of the light in LNOI optical circuits are important. Polarization elements of interest include polarizers, polarization beam splitters (PBS), and polarization converters and rotators.

Saitoh et al.<sup>[100]</sup> showed that it is possible to design TE-pass and TM-pass polarizer in LNOI using ridge waveguides by varying the waveguide dimensions. The function of the polarizer is realized by radiating the unwanted polarization in the slab waveguide, which is based on the lateral leakage of the ridge waveguide.<sup>[101]</sup> The lateral leakage takes place when the waveguide mode of the ridge waveguide is phase matched to a laterally propagating slab mode, which propagates under a certain angle. The use of this effect in LNOI waveguides resulted in simulated extinction ratios of 108 dB/mm and 27 dB/mm for TE-pass and TM-pass polarizers, respectively.

Polarization beam splitters have been designed and simulated in LNOI. Duan et al.<sup>[102]</sup> showed in their simulations that a negative refractive photonic crystals can be used to separate the different polarizations. However, the suggested device uses slab modes to excite the photonic crystal, creating challenges for on chip integration. Furthermore, the holes in such photonic crystals can introduce significant scattering losses due to the fabrication tolerances, which makes this solution not very attractive. More attractive is the design suggested by Gong et al.,<sup>[103]</sup> who use a directional coupler based design to achieve a PBS. Their simulations suggest that an extinction ratio of 35 dB between the two polarizations is possible. However, there are more polarization beam splitter designs that might be interesting to realize

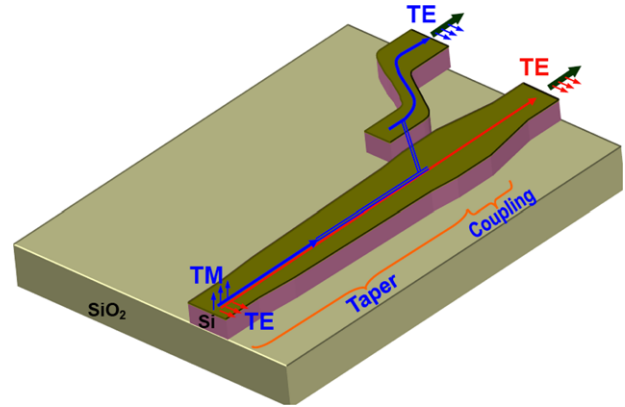


**Figure 13.** Schematic configuration of the proposed polarization splitter-rotator based on an asymmetrical directional coupler. Reproduced with permission.<sup>[105]</sup> Copyright 2011, Optical Society of America.

in the LNOI platform, which have already been demonstrated in silicon-based optical platforms. A nice overview of such devices is given by Dai et al.<sup>[104]</sup> Of particular interest is a polarization beam splitter-rotator that converts a TM input mode to  $TE_1$  mode that can be coupled to a neighboring waveguide via an asymmetrical directional coupler, so that two fundamental TE modes are leaving this device as it is illustrated in **Figure 13**.<sup>[105]</sup> This enables polarization multiplexing approaches on chip, where both arms can be manipulated by nonlinear optical or electro optical elements.

On-chip electrical controllable TE/TM polarization converters have been demonstrated using diffused waveguides in lithium niobate, employing the  $r_{51}$  electro-optical coefficient and phase-matching grating electrodes.<sup>[106]</sup> Such TE/TM polarization converters have also been demonstrated in ion-sliced lithium niobate, showing that it can be realized in LNOI. This might be especially interesting as the thin-film lithium niobate enhances the electric field overlap with the optical waveguide mode, which increases the efficiency.<sup>[107]</sup>

## 2.7. Gain Elements

Rare earth elements such as erbium and thulium have successfully been diffused in lithium niobate crystals to achieve optical gain media. In the past, such optical gain devices have mainly been fabricated in titanium diffused waveguides, where the erbium was diffused first into the lithium niobate at  $\approx 1000$  to  $1130$  °C for  $\approx 100$  to  $150$  h, before the titanium waveguide was fabricated.<sup>[108]</sup> This has led to the development of optical amplifiers<sup>[109,110]</sup> and laser<sup>[111,112]</sup> on lithium niobate chips at telecommunication wavelengths. Similar elements are also very interesting for LNOI waveguides, as they would enable a higher functionality including devices such as amplifier and laser light sources on chip. However, doping lithium niobate with rare earth elements by a diffusion process may need to be completed before the lithium niobate thin film is bonded on the silica buffer layer as the high diffusion temperatures would destroy the bonding layer.<sup>[29]</sup> A potential alternative would be the local implantation of rare earth ions in combination with a low temperature ( $500$  °C)

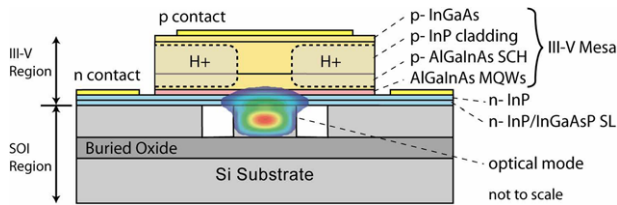


**Figure 14.** Schematic drawing of the hybrid laser structure on SOI with the optical mode superimposed. Reproduced with permission.<sup>[114]</sup> Copyright 2006, Optical Society of America.

annealing step.<sup>[113]</sup> This indicates that further investigations are necessary to achieve such gain elements on LNOI wafers.

Another option to achieve on-chip lasers is the heterogeneous integrate of electrically pumped evanescent lasers on LNOI waveguides. Such lasers have successfully been demonstrated on SOI, as it is illustrated in **Figure 14**.<sup>[114]</sup> A similar heterogeneous integration of III-V lasers should also be possible on LNOI and needs to be investigated in the near future. Special care needs to be taken as LNOI has a lower refractive index compared to SOI waveguides.

## 2.8. Photodetectors

Photodetectors have been investigated early on in lithium niobate. W. K. Chan et al. demonstrated in 1989 a GaAs photodetector integrated with lithium niobate waveguides for the detection of red laser light.<sup>[115–117]</sup> After this initial demonstration, no significant progress was made to investigate and develop photodetectors for lithium niobate waveguides further. This can probably be attributed to the rise of silicon photonics and the ability to integrate many optical components, such as photodetectors, on the same chip. Now, LNOI offers a similar optical integration density, which makes the development of photodetectors for LNOI waveguides attractive. This means that many of the well-established heterogeneous integration fabrication capabilities of III-V photodetectors on silicon based platforms should be transferable to LNOI waveguides.<sup>[118–120]</sup> Such heterogeneous photodetectors are very attractive as they can have high bandwidths, such as the recent demonstration of 65 GHz bandwidth high-power photodetectors.<sup>[121]</sup> This shows that further investigations are necessary to have photodetectors available on LNOI waveguides.

Single photon detectors on titanium indiffused lithium niobate waveguides have recently been demonstrated, showing that also detectors for quantum optical applications are feasible when lithium niobate is used as a material platform.<sup>[122,123]</sup> The higher confinement of the optical mode in LNOI waveguides will increase the optical field overlap with the single photon detector, benefiting the photon absorption probability.

## 3. Emerging and Potential Future Applications

The previous section introduced different building blocks that are interesting in order to achieve highly functional PICs in LNOI. In this section, these building blocks will be taken into the context of

telecommunication, quantum optics and visible wavelength photonics to discuss how the building blocks in LNOI can achieve attractive functionalities in these fields. The motivation of this section is to give an overview of what is possible with LNOI and where potential attractive applications are without claiming to give a complete list.

### 3.1. Telecommunication

LNOI is a very attractive platform for telecommunication applications as LNOI provides the ability to integrate fast electro optical modulators and efficient nonlinear optical elements on the same chip. In the following some interesting telecommunication applications for LNOI PICs are given.

#### 3.1.1. IQ Modulator

For decades, diffused waveguide based lithium niobate modulators were one of the standard optical modulators in telecommunication applications. As indicated in *section 2.3*, lithium niobate modulators in LNOI can achieve very high modulation frequencies with moderately low voltage-length product ( $V_{\pi}L$ ). The low voltage-length product can be important in both the energy consumption of the device, but also in allowing for compact device size. At 1.5 Vcm,<sup>[56]</sup> LNOI modulators can be envisaged to have the same compact dimensions as the InP modulators that are now displacing traditional in-diffused LN waveguide based modulators in coherent optical transceivers.<sup>[124,125]</sup> Moreover, the fast response time of LNOI modulators (up to 110 GHz<sup>[76]</sup>) make their modulation bandwidth more than sufficient for future 400 Gb/s channels running at over 60 Gbaud,<sup>[126]</sup> and may prove to be a key enabler for terabit-per-second channels.<sup>[127]</sup>

In modern, high-capacity optical communications systems, dual-nested Mach-Zehnder modulators enable full field modulation, allowing for spectrally efficient modulation of light waves using quadrature-amplitude modulation. A schematic of such a circuit is given in **Figure 15b**. Further, it is possible to integrate an optical equalizer on the same chip to improve the optical signal-to-noise ratio (OSNR).<sup>[128,129]</sup>

#### 3.1.2. Wavelength Converters

Nonlinear optical elements are very attractive for telecommunication applications as they allow a variety of interesting applications such as the transfer of signals from one wavelength to another without the need of going via the electrical domain, thus reducing the network operational cost, energy consumption and electronic processing latencies. Examples of such wavelength converters are the generation of optical phase conjugation to correct nonlinear phase noise accumulated along fibers<sup>[130]</sup> and optical multicasting to deliver the same data to numerous customers.<sup>[131]</sup> Realizing such systems on LNOI is very attractive as conversion efficiencies of 1600%  $W^{-1}cm^{-2}$  are predicted in LNOI waveguides,<sup>[28]</sup> reducing the pump power necessary for the nonlinear optical processes and achieving nonlinear optical

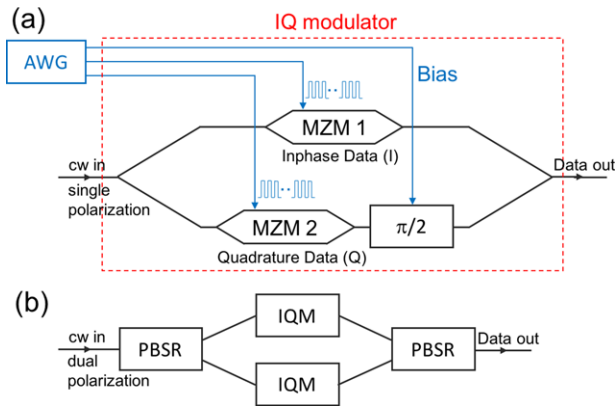


**Figure 15.** a) Schematic illustration of an IQ modulator, consisting out of two Mach-Zehnder modulators (MZM) and a  $\pi/2$  phase shifter in the lower arm of the IQ modulator. b) Polarization multiplexed IQ modulator, where a polarization beam splitter-rotator (PBSR), as show in Figure 14, splits and rotates the two polarizations at the input as well as combines them after the IQ modulators.

signal amplification on chip.<sup>[132]</sup> The nonlinear optical process that takes place in the periodically poled waveguides is that the pump wavelength gets frequency doubled, generating a second harmonic, which in turn acts as a pump for a stimulated difference frequency generation (DFG) process, generating the phase conjugated idler. As the second order nonlinear DFG process relies on quasi-phase matching, wavelength conversion in lithium niobate avoids nonlinear cross-talk issues that impair other well-explored platforms that exploit third order nonlinear effects.<sup>[133]</sup>

The photorefractive effect, which can result in optical damage, relaxes two to three orders of magnitude faster in LNOI<sup>[134]</sup> compared to bulk lithium niobate. This together with the strongly guided optical waveguide modes makes LNOI waveguides more resistant to optical damage. This can be explained by the fact that the refractive index change caused by the photorefractive effect is relatively small compared to the refractive index contrast of a single mode waveguide in LNOI, which significantly reduced the risk of the optical mode distortion due to the photorefractive effect. This may render heating of lithium niobate waveguides for high power applications unnecessary with potential benefits in terms of energy efficiency and simplified packaging. However, further investigations may be required in order to be conclusive on this. Such systems can be made even more attractive by adding more functionality on chip such as polarization diversity and filtering of the pump wavelength. This can be achieved by on-chip

polarization beam splitter-rotator and an additional nonlinear element in parallel as well as a Bragg grating or ring resonator for filtering the pump wavelength.<sup>[135]</sup> The proposed PIC is illustrated in Figure 16.

### 3.1.3. Comb Sources

The generation of frequency combs has attracted significant attention in the last decades as they found applications in frequency metrology, optical clocks, and precision navigation among others.<sup>[136,137]</sup> Coherent comb sources are particularly interesting for high speed communication as phase stable laser light sources are required for advanced modulation formats and Kerr frequency comb sources, for example in SiN, have been successfully used for such applications.<sup>[138,139]</sup> Comb sources have also been theoretically investigated in lithium niobate in the structure of a microdisk resonator<sup>[140]</sup> and ring resonators.<sup>[141]</sup> This promises to be very exciting as lithium niobate has a high optical nonlinearity and the spectral behavior of the resonators can be designed by using QPM structures with a certain period in the resonator. When X-cut LNOI samples are used, the QPM structure can only be along Y-propagating waveguides as the crystal Z-direction gets inverted, this limitation can be accommodated by using race track resonator geometry, where the straight sections are Y-propagating and can be periodically poled (see Figure 17a). This configuration also allows the use of coplanar electrodes on the other side of the race track resonator, which can be used to match a fundamental resonance wavelength of the resonator with the wavelength that is phase matched with the QPM structure. Furthermore, one has to ensure that both, the fundamental and the second harmonic wavelength, are resonant in the racetrack. The nonlinear process that takes place in the resonator is that the pump wavelength gets frequency doubled, generating the second harmonic. The second harmonic acts as a pump for difference frequency generation processes that matches the free spectral range (FSR) of the resonator, generating a frequency comb.<sup>[141]</sup> The comb lines themselves may generate even more wavelengths near both the fundamental and harmonic via SHG and SFG processes. The nonlinear optical processes are illustrated in Figure 17b. Such comb sources can be pumped by on-chip lasers, reducing any coupling losses that might occur. Furthermore, it is possible to natively integrate comb sources with high speed modulators on LNOI, which is attractive as coupling losses between different platforms can be avoided.

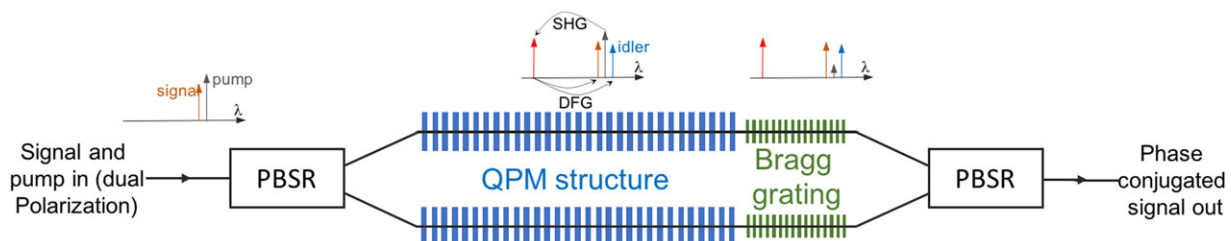


**Figure 16.** Proposed nonlinear optical circuit that can be used for optical phase conjugation and optical multicasting that uses polarization multiplexed signals, which get separated by polarization beam splitter-rotator (PBSR), as show in Figure 13, to split and rotate the two polarizations at the input as well as combines them after the nonlinear optical elements and the Bragg filters to suppress the pump wavelength.

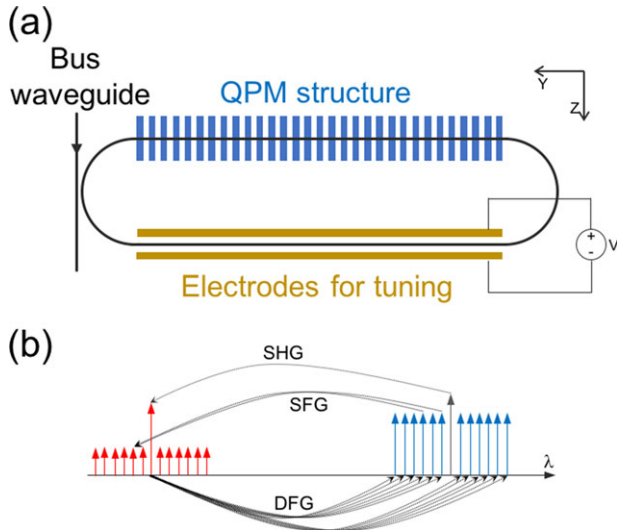


**Figure 17.** a) Race track resonator with QPM structure in one straight section for the nonlinear optical process and electrodes on the other straight section for tuning one resonance wavelength to the wavelength that is phase matched in the QPM structure. b) Illustration of the nonlinear optical processes that take place in the resonator. The pump wavelength (grey arrow) gets frequency doubled. The frequency doubled light acts then as a pump for difference frequency generation (DFG) processes, that generate wavelengths that match the FSR of the resonator, generating a frequency comb around the initial pump wavelength. The frequency comb itself might generate even further wavelengths around the frequency doubled wavelength via sum frequency generation (SFG) and second harmonic generation (SHG) processes.

### 3.2. Quantum Optics

Lithium niobate is an attractive material for quantum optical applications. A detailed overview of work, which used lithium niobate crystals for quantum optical application is given by Alibart et al.<sup>[142]</sup> Most of the reviewed work by Alibart et al.<sup>[142]</sup> used lithium niobate only as a photon source for quantum applications. However, integrating more optical elements on the same platform would be highly beneficial as it reduces coupling losses and increases the operation stability, enabling operations involving photon interference with minimal decoherence. This

makes LNOI a very attractive platform for quantum optical PICs, as it offers low loss optical waveguides, high integration density, integration of nonlinear optical elements for quantum light sources and the integration of ultra-fast electro-optical modulators on the same platform. The following lists only a few attractive applications for quantum optical applications in LNOI.

#### 3.2.1. Photon Pair Sources

One of the most popular methods for generating quantum light is the entangled photon pair generation via spontaneous parametric down conversion (SPDC), which is a nonlinear optical process, converting high energy photons into pairs of low energy photons. Such SPDC sources can under certain conditions create a particularly interesting state of quantum light, which is a heralded spectrally pure single photon.<sup>[143,144]</sup> Therefore, it is highly desirable to be able to generate such heralded spectrally pure single photons in the platform of LNOI.

As described above, efficient nonlinear optical elements can be engineered in LNOI by periodically inverting the crystal direction applying the QPM method. With the ability of achieving very short domain inversion periods in LNOI,<sup>[81]</sup> it should be possible to generate SPDC sources with counter-propagating photon pairs in LNOI. The phase matching function of such a QPM structure is illustrated in Figure 18b. If this phase matching function is multiplied by a standard spectral pump envelop (Figure 18a), then the resulting joint spectral amplitude (Figure 18c), shows minimal spectral correlations within each photon-pair, resulting in a high spectral purity.<sup>[145]</sup> A heralded spectrally pure single photon can be achieved by detecting the other photon of the pair. Such single photon sources are highly interesting as they could be used for on-chip quantum optical applications such as boson sampling.<sup>[146]</sup>

#### 3.2.2. Single Photon Wavelength Converters

Historically, wavelength conversion by using nonlinear optical elements was attractive for up-converting single photons from communication wavelengths to single photons at visible

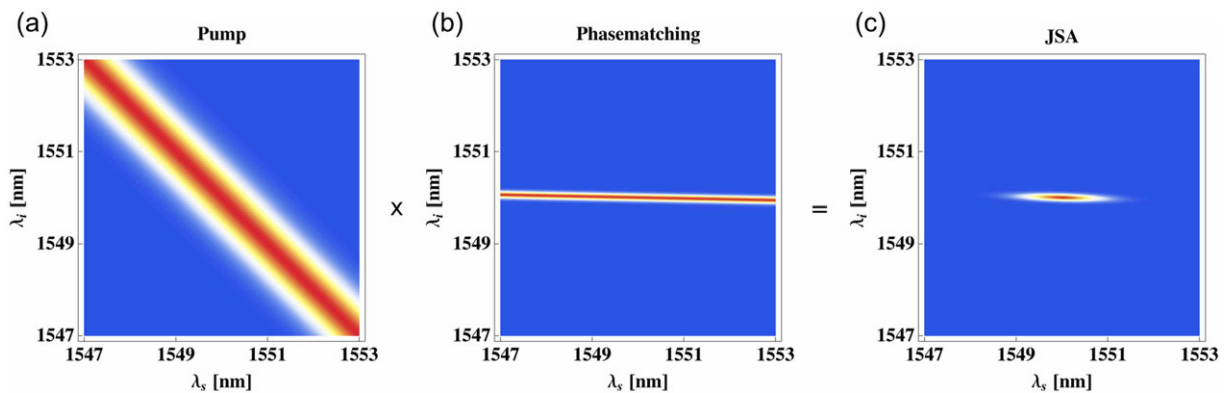


**Figure 18.** Pump envelope, phase matching function and joint spectral amplitude (JSA) plotted in the Gaussian approximation without phase. Reproduced with permission.<sup>[145]</sup> Copyright 2009, Optical Society of America.

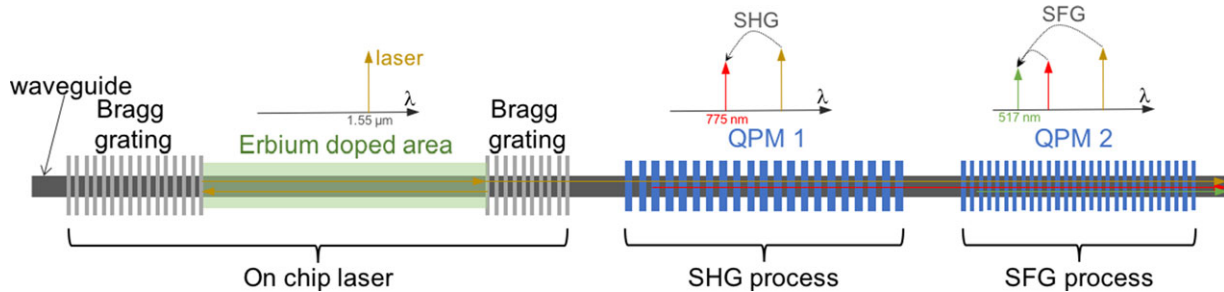


**Figure 19.** Illustration of green laser light source integrated on chip by using two cascaded nonlinear optical processes to up convert the laser light from the erbium doped on chip laser.

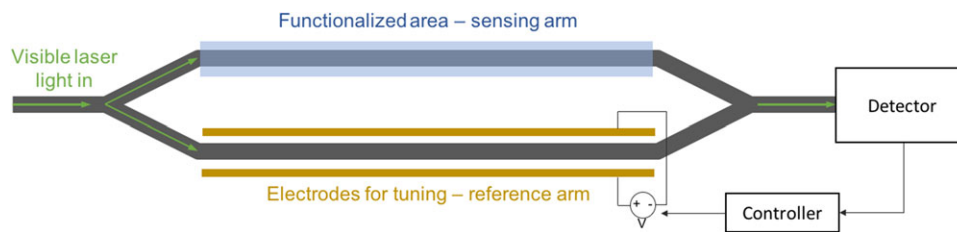


**Figure 20.** Illustration of a MZI that uses one arm as a sensing arm. The refractive index change due to adhering biomarkers in the sensing arm is compensated by measuring the output power of the MZI and adjusting the voltage in the reference arm accordingly, to enable a working point at the highest sensitivity.

wavelengths. This was the case as single photon detectors had a low detection efficiency in the past and suffered from large dark counts at communication wavelengths.<sup>[147,148]</sup> Recent progresses in the development of highly efficient single photon detectors at communication wavelengths<sup>[149–151]</sup> makes the up-conversion of single photons not necessary. However, wavelength converters are still attractive as they can convert single photons from quantum dots or ion traps, which usually emit in the ultraviolet to near infrared wavelength regime, to single photons at communication wavelengths. Such wavelength converters enable long distance quantum state transfer from flying qubit to a stationary qubit or vice versa, and entanglement distribution between two remote matter qubits in long-distance quantum networks.<sup>[152–154]</sup> The high conversion efficiencies that are achievable in LNOI,<sup>[28]</sup> makes this platform very attractive for such wavelength down conversion schemes and the integration of quantum dots in such waveguides seems also feasible.<sup>[155]</sup>

### 3.2.3. Quantum Memory

Quantum memories will be an essential element for future long-range quantum communication networks, by enabling the synchronization of the flow through the communication network by holding the quantum information until it is needed. The holding of the quantum information can be achieved by mapping the quantum state of light to quantum transitions of a material system, whereas the reverse process can be used for releasing the quantum information. Erbium and thulium doped lithium niobate waveguides have successfully been used to store the quantum information of light in the nanosecond to microsecond time scale, by using the photon-echo protocol.<sup>[156–159]</sup> This shows great

promise that similar quantum memories can also be established in LNOI, as the lithium niobate can locally be doped with erbium or thulium before the lithium niobate thin film is bonded onto the silica buffer layer in the LNOI wafer fabrication process.

## 3.3. Visible and Mid-IR Wavelength Photonics

Lithium niobate and silicon nitride are both transparent at the visible and Mid-IR wavelength regime, which makes wire and ridge waveguides in LNOI attractive for visible and Mid-IR wavelength photonic application such as biophotonics. Lithium niobate is also resistant to most chemicals, which makes the functionalization of the surface for biophotonic application feasible.<sup>[160]</sup> Furthermore, one can expect that many of the functionalization techniques that were developed for surface acoustic wave biosensors on lithium niobate and lithium tantalate,<sup>[161]</sup> can be transferred to the LNOI platform. Ridge waveguides have recently been demonstrated in LNOI with a loss of  $4 \pm 2$  dB/cm at a wavelength of 674 nm.<sup>[162]</sup> In the following, we give examples of some interesting optical elements for biophotonic applications.

### 3.3.1. Visible Wavelength Converters

Visible light sources on chip are difficult to integrate, resulting in the use of grating couplers or butt coupling to couple laser light into the biophotonic integrated circuits.<sup>[163]</sup> LNOI offers the possibility to generate a nearly arbitrary range of visible wavelength signals on chip by using nonlinear optical elements and

designing the quasi-phase matching period appropriately. It has already been demonstrated that 1530 nm laser light can be efficiently frequency doubled on chip to generate light with a wavelength of 765 nm.<sup>[28]</sup> Similarly, one can also think of generating other wavelength using SHG, SFG and DFG and combinations of these processes. For example, one can generate green light by first frequency doubling 1550 nm laser light, which will generate 775 nm light, followed by a cascaded sum frequency process of 1550 nm and 775 nm light to generate a wavelength of 517 nm. A schematic of such a system with an integrated erbium doped laser is illustrated in **Figure 19**. Even more attractive might be to use an heterogeneous integrated electrically pumped evanescent laser as a pump for the nonlinear optical processes.<sup>[114]</sup> Another alternative to generate visible wavelengths are nonlinear optical resonant structures such as ring resonators.<sup>[140]</sup>

Similarly, one can generate Mid-IR wavelength in LNOI waveguides by a stimulated DFG process. This makes this platform also interesting for typical Mid-IR such as gas sensing or blood sugar sensing.<sup>[164]</sup>

### 3.3.2. Tracking Mach-Zehnder Interferometer

Mach-Zehnder interferometers are an attractive and very sensitive configuration for biophotonic sensors.<sup>[163]</sup> One arm of the Mach-Zehnder interferometer is thereby exposed to the biological specimen, whereas the other arm acts as a reference arm. The power at the output of the Mach-Zehnder interferometer can then be used to determine the refractive index change in the measuring arm, which follows a sinusoidal function.

An attractive way to achieve a linear measurement system that works at the highest sensitivity point of the MZI, is by fabricating the MZI in LNOI and using electrodes at the reference arm of the MZI as illustrated in **Figure 20**. The electrodes can then be used to induce a refractive index change in the reference arm that maps the refractive index change of the sensing arm by applying a voltage to the electrodes. The applied voltage induces thereby a refractive index change via the electro-optical effect in LNOI. The applied voltage can then be used as a linear measurement of the refractive index change in the measurement arm, making it a simple and attractive solution for biophotonic applications.

## 4. Conclusion

The recent developments in the integrated optical platform lithium niobate on insulator (LNOI) were reviewed. It has been shown that many of the key building blocks for highly integrated photonic integrated circuits (PICs) have been established on this platform including low loss optical waveguides, electro-optical interfaces for ultra-fast modulation, nonlinear optical elements and resonators.

However, further work needs to be done to make LNOI an attractive and competitive integrated optical platform. (i) This includes improved optical interfacing to LNOI waveguides, reducing the fiber to chip coupling losses for example by developing inverted tapers and waveguide tapers on LNOI. (ii) The nonlinear optical elements that have been established in this platform have

shown a nonlinear optical efficiency of  $160\% \text{ W}^{-1} \text{ cm}^{-2}$ . However, simulations indicate that the nonlinear optical efficiency should be an order of magnitude higher in this platform.<sup>[28]</sup> The reasons for the lower experimentally achieved efficiencies needs to be investigated. (iii) Polarization rotating and controlling elements need to be further investigated and experimentally demonstrated as most of the polarization elements so far have only been simulated. Furthermore, for telecommunication applications it would be very attractive to use polarization beam splitter-rotators (**Figure 13**) in LNOI as it enables polarization multiplexing. (iv) Optical gain media need to be demonstrated in this platform, either via bonding already doped lithium niobate in the LNOI wafer fabrication process, or by doping the LNOI wafer after fabrication using ion implantation techniques. Also, the heterogeneous integration of III-V lasers on LNOI waveguides needs to be investigated. (v) The development of photodetectors on LNOI waveguides requires further investigation. Integrated photodetectors will be very important for future PIC applications as it increases the device stability and eliminated additional coupling losses.

We also gave a brief overview of some interesting applications of LNOI PICs in the field of telecommunication, quantum photonics and visible and Mid-IR wavelength photonics. In telecommunications, we suggested the use of high speed electrodes in LNOI for IQ modulators, highly efficient nonlinear optical wavelength converters and comb sources. In quantum photonics, some interesting applications are the use of nonlinear optical elements in LNOI for pure heralded photon sources, single photon wavelength converters and rare earth doped LNOI as a quantum memory. In the field of visible wavelength photonics, the use of LNOI circuits for visible wavelength light sources on chips and as biosensors in refractive index tracking Mach-Zehnder interferometer might be interesting applications and the potential to create combs of coherent light at visible wavelength presents some exciting sensing and imaging opportunities.

From this review, the potential benefits of LNOI are clear, however, it is worth considering whether LNOI will be widely adopted as a fundamental platform for photonic integration, or whether sufficient benefits could be achieved by hybrid integrating local islands of  $\text{LiNbO}_3$  onto a more mature wafer platform such as SiN and SOI. The extremely low loss ( $2.7 \text{ dB m}^{-1}$ )<sup>[51]</sup> and the tight waveguide bending radii available in the LNOI platform are comparable to well established SiN platforms, so there is no compromise in terms of insertion loss and device compactness to take advantage of the strong electro-optic and nonlinear optical properties of LN. This virtuous combination of properties has maintained the industrial relevance of diffused lithium niobate waveguides for decades, strongly suggesting that LNOI will become an important and potentially widely used PIC platform in the near future. The major drawback of LNOI is the limitations of wafer sizes and high cost per wafer; however as discussed, there are few fundamental obstacles that would prevent LNOI wafers to scale in a similar manner to SOI wafers, as they share a very similar manufacturing method. Thus, larger wafer sizes, lower cost and maturing manufacturing tolerances should develop as the community adopts this platform. We see no reason why the LNOI platform could not become a major wafer platform for PICs. Overall it can be concluded that LNOI is still a rapidly developing platform and more optical elements need to be experimentally



demonstrated in this platform. The potential to integrate sources and detectors with this platform presents a tantalizing vision for a truly integrated photonic system on a chip.

## Acknowledgements

The authors would like to acknowledge the support by the Australian Research Council (CE110001018) and by the Defense Advanced Research Projects Agency DODOS program. The authors thank Nicholas Volet for assistance and Benjamin Soffe for drawing Figure 1.

## Conflict of Interest

The authors declare no conflict of interest.

## Keywords

integrated photonics, lithium niobate, nonlinear optics, optoelectronics, photonic integrated circuits

Received: September 25, 2017

Revised: January 15, 2018

Published online: February 23, 2018

- 
- [1] B. Jalali, S. Fathpour, *J. Lightwave Technol.* **2006**, *24*, 4600.
- [2] J. Leuthold, C. Koos, W. Freude, *Nature Photonics* **2010**, *4*, 535.
- [3] L. Pavesi, *J. Phys.: Condens. Matter* **2003**, *15*, R1169.
- [4] A. E.-J. Lim, J. Song, Q. Fang, C. Li, X. Tu, N. Duan, K. K. Chen, R. P.-C. Tern, T.-Y. Liow, *IEEE J. Select. Topics Quantum Electron.* **2014**, *20*, 405.
- [5] C. G. H. Roeloffzen, L. Zhuang, C. Taddei, A. Leinse, R. G. Heide- man, P. W. L. van Dijk, R. M. Oldenbeuving, D. A. I. Marpaung, M. Burla, K. J. Boller, *Opt Express* **2013**, *21*, 22937.
- [6] D. J. Moss, R. Morandotti, A. L. Gaeta, M. Lipson, *Nature Photonics* **2013**, *7*, 597.
- [7] W. D. Sacher, Y. Huang, G.-Q. Lo, J. K. S. Poon, *J. Lightwave Technol.* **2015**, *33*, 901.
- [8] R. Nagarajan, M. Kato, D. Lambert, P. Evans, *Semicond. Sci. Technol.* **2012**, *27*, 094003.
- [9] F. A. Kish, D. Welch, R. Nagarajan, J. L. Pleumeekers, V. Lal, M. Ziari, A. Nilsson, M. Kato, S. Murthy, P. Evans, S. W. Corzine, M. Mitchell, P. Samra, M. Missey, S. DeMars, R. P. Schneider, M. S. Reffle, T. Butrie, J. T. Rahn, M. Van Leeuwen, J. W. Stewart, D. J. Lambert, R. C. Muthiah, H. Tsai, J. S. Bostak, A. Dentai, K. Wu, H. Sun, D. J. Pavinski, J. Zhang, J. Tang, J. McNicol, M. Kuntz, V. Dominic, B. D. Taylor, R. A. Salvatore, M. Fisher, A. Spannagel, E. Strzelecka, P. Studenkov, M. Raburn, W. Williams, D. Christini, K. K. Thomson, S. S. Agashe, R. Malendevich, G. Goldfarb, S. Melle, C. Joyner, M. Kauf- man, S. G. Grubb, *IEEE J. Select. Topics Quantum Electron.* **2011**, *17*, 1470.
- [10] R. Nagarajan, M. Kato, J. Pleumeekers, P. Evans, S. Corzine, S. Hurtt, A. Dentai, S. Murthy, M. Missey, R. Muthiah, R. A. Salvatore, C. Joyner, R. Schneider, M. Ziari, F. Kish, D. Welch, *IEEE J. Select. Topics Quantum Electron.* **2010**, *16*, 1113.
- [11] E. H. Turner, *Appl. Phys. Lett.* **1966**, *8*, 303.
- [12] A. M. Prokhorov, Y. S. Kuzminov, *Physics and Chemistry of Crystalline Lithium Niobate*, Hilger, IOP Publishing Ltd, Bristol, BS1 6NX, Eng- land **1990**.
- [13] M. Bazzan, C. Sada, *Appl. Phys. Rev.* **2015**, *2*, 040603.
- [14] P. Ganguly, J. C. Biswas, S. K. Lahiri, *Opt Commun* **1998**, *155*, 125.
- [15] J. D. Witmer, J. A. Valery, P. Arrangoiz-Arriola, C. J. Sarabalis, J. T. Hill, A. H. Safavi-Naeini, *Sci. Rep.* **2017**, *7*, 46313.
- [16] J. D. Witmer, J. T. Hill, A. H. Safavi-Naeini, *Opt Express* **2016**, *24*, 5876.
- [17] L. Chen, J. Chen, J. Nagy, R. M. Reano, *Opt Express* **2015**, *23*, 13255.
- [18] L. Chen, Q. Xu, M. G. Wood, R. M. Reano, *Optica* **2014**, *1*, 112.
- [19] L. Chen, M. G. Wood, R. M. Reano, *Opt Express* **2013**, *21*, 27003.
- [20] L. Cao, A. Aboketaf, Z. Wang, S. Preble, *Opt Commun* **2014**, *330*, 40.
- [21] P. O. Weigel, M. Savanier, C. T. DeRose, A. T. Pomerene, A. L. Star- buck, A. L. Lentine, V. Stenger, S. Mookherjea, *Sci. Rep.* **2016**, *6*, 22301.
- [22] J. Chiles, S. Fathpour, *Optica* **2014**, *1*, 350.
- [23] D. Liang, G. Roelkens, R. Baets, J. E. Bowers, *Materials* **2010**, *3*, 1782.
- [24] G. Roelkens, L. Liu, D. Liang, R. Jones, A. Fang, B. Koch, J. Bowers, *Laser & Photon. Rev.* **2010**, *4*, 751.
- [25] L. Chang, M. H. P. Pfeiffer, N. Volet, M. Zervas, J. D. Peters, C. L. Manganelli, E. J. Stanton, Y. Li, T. J. Kippenberg, J. E. Bowers, *Opt Lett* **2017**, *42*, 803.
- [26] P. O. Weigel, S. Mookherjea, *Optical Materials* **2017**, *66*, 605.
- [27] G. Poberaj, H. Hu, W. Sohler, P. Günter, *Laser & Photon. Rev.* **2012**, *6*, 488.
- [28] L. Chang, Y. Li, N. Volet, L. Wang, J. Peters, J. E. Bowers, *Optica* **2016**, *3*, 531.
- [29] S. Li, L. Cai, Y. Wang, Y. Jiang, H. Hu, *Opt Express* **2015**, *23*, 24212.
- [30] L. Cai, Y. Wang, H. Hu, *Opt Commun* **2017**, *387*, 405.
- [31] L. Cai, Y. Wang, H. Hu, *Opt Lett* **2015**, *40*, 3013.
- [32] L. Cai, S. L. H. Han, H. Hu, *Opt Express* **2015**, *23*, 1240.
- [33] L. Cai, R. Kong, Y. Wang, H. Hu, *Opt Express* **2015**, *23*, 29211.
- [34] S. Kurimura, Y. Kato, M. Maruyama, Y. Usui, H. Nakajima, *Appl. Phys. Lett.* **2006**, *89*, 191123.
- [35] M. F. Volk, S. Sunstov, C. E. Rüter, D. Kip, *Opt Express* **2016**, *24*, 1386.
- [36] N. Courjal, B. Guichardaz, G. Ulliac, J.-Y. Rauch, B. Sadani, H.-H. Lu, M.-P. Bernal, *J. Phys. D: Appl. Phys.* **2011**, *44*, 305101.
- [37] R. Takigawa, E. Higurashi, T. Kawanishi, T. Asano, *Opt Express* **2014**, *22*, 27733.
- [38] H. Hu, R. Ricken, W. Sohler, R. B. Wehrspohn, *IEEE Photon. Technol. Lett.* **2007**, *19*, 417.
- [39] H. Hui, R. Ricken, W. Sohler, ECIO Conference **2008**, 75.
- [40] J. Deng, G. Si, A. J. Danner, Photonics Global Conference (PGC) **2010**.
- [41] C. M. Chang, C. S. Yu, F. C. Hsieh, C. T. Lin, P. H. Lin, J. S. Kao, T. T. Huang, C. N. Hsiao, M. H. Shiao, 10th IEEE International Con- ference on Nano/Micro Engineered and Molecular Systems **2015**, 485.
- [42] H. Hu, R. Ricken, W. Sohler, *Opt Express* **2009**, *17*, 24261.
- [43] S. Y. Siew, S. S. Saha, M. Tsang, A. J. Danner, *IEEE Photon. Technol. Lett.* **2016**, *28*, 573.
- [44] G. Ulliac, V. Calero, A. Ndao, F. I. Baida, M.-P. Bernal, *Optical Mate- rials* **2016**, *53*, 1.
- [45] C. Wang, X. Xiong, N. Andrade, V. Venkataraman, X.-F. Ren, G.-C. Guo, M. Lončar, *Opt Express* **2017**, *25*, 6963.
- [46] H. Nagata, N. Mitsugi, K. Shima, M. Tamai, *Journal of Crystal Growth* **1998**, *187*, 573.
- [47] K. Shima, N. Mitsugi, H. Nagata, *J. Mater. Res.* **1998**, *13*, 527.
- [48] H. Hu, A. P. Milenin, R. B. Wehrspohn, H. Hermann, W. Sohler, *Journal of Vacuum Science & Technology a: Vacuum, Surfaces, and Films* **2006**, *24*, 1012.
- [49] I. Krasnokutskaja, J. Tambasco, X. Li, A. Peruzzo, *Opt Express* **2018**, *26*, 313745.
- [50] C. Wang, M. Zhang, B. Stern, M. Lipson, M. Lončar, arXiv **arXiv:1701.06470v1**, **2017**.
- [51] M. Zhang, C. Wang, R. Cheng, A. Shams-Ansari, M. Lončar, *Optica* **2017**, *4*, 1536.

- [52] L. Cai, S. Zhang, H. Hu, *J. Opt.* **2016**, *18*, 035801.
- [53] R. Geiss, S. Saravi, A. Sergeev, S. Diziain, F. Setzpfandt, F. Schrempe, R. Grange, E.-B. Kley, A. Tünnermann, T. Pertsch, *Opt Lett* **2015**, *40*, 2715.
- [54] A. Rao, M. Malinowski, A. Honardoost, J. R. Talukder, P. Rabiei, P. Delfyett, S. Fathpour, *Opt Express* **2016**, *24*, 29941.
- [55] S. Jin, L. Xu, H. Zhang, Y. Li, *IEEE Photon. Technol. Lett.* **2016**, *28*, 736.
- [56] P. Rabiei, J. Ma, S. Khan, J. Chiles, S. Fathpour, *Opt Express* **2013**, *21*, 25573.
- [57] A. Rao, A. Patil, J. Chiles, M. Malinowski, S. Novak, K. Richardson, P. Rabiei, S. Fathpour, *Opt Express* **2015**, *23*, 22746.
- [58] D. Taillaert, W. Bogaerts, P. Bienstman, T. F. Krauss, P. Van Daele, I. Moerman, S. Verstyuyft, K. De Mesel, R. Baets, *IEEE J. Quantum Electron.* **2002**, *38*, 949.
- [59] D. Taillaert, F. Van Laere, M. Ayre, W. Bogaerts, D. Van Thourhout, P. Bienstman, R. Baets, *Jpn. J. Appl. Phys.* **2006**, *45*, 6071.
- [60] M. Mahmoud, S. Ghosh, G. Piazza, CLEO: Science and Innovations, CLEO-SI 2015, **2015**.
- [61] Z. Chen, Y. Wang, Y. Jiang, R. Kong, H. Hu, *Optical Materials* **2017**, *72*, 136.
- [62] H. Zhang, C. Li, X. Tu, X. Luo, M. Yu, P. G.-Q. Lo, *Appl. Phys. A* **2013**, *115*, 79.
- [63] C. R. Doerr, L. Chen, Y.-K. Chen, L. L. Buhl, *IEEE Photon. Technol. Lett.* **2010**, *22*, 1461.
- [64] G. Maire, L. Vivien, G. Sattler, A. Kaźmierczak, B. Sanchez, K. B. Gylfason, A. Griol, D. Marris-Morini, E. Cassan, D. Giannone, H. Söhlström, D. Hill, *Opt Express* **2008**, *16*, 328.
- [65] T. Shoji, T. Tsuchizawa, T. Watanabe, K. Yamada, H. Morita, *Electron. Lett.* **2002**, *38*, 1669.
- [66] T. Wahlbrink, W. S. Tsai, M. Waldow, M. Först, J. Bolten, T. Mollenhauer, H. Kurz, *Microelectronic Engineering* **2009**, *86*, 1117.
- [67] V. Nguyen, T. Montalbo, C. Manolatu, A. Agarwal, C.-Y. Hong, J. Yasaitis, L. C. Kimerling, J. Michel, *Appl. Phys. Lett.* **2006**, *88*, 081112.
- [68] B. Ben Bakir, A. V. de Gyves, R. Orobitchouk, P. Lyan, C. Porzier, A. Roman, J. M. Fedeli, *IEEE Photon. Technol. Lett.* **2010**, *22*, 739.
- [69] L. Chen, C. R. Doerr, Y.-K. Chen, T.-Y. Liow, *IEEE Photon. Technol. Lett.* **2010**, *22*, 1744.
- [70] G. Kurczveil, P. Pintus, M. J. R. Heck, J. D. Peters, J. E. Bowers, *IEEE Photonics J.* **2013**, *5*, 6600410.
- [71] M. L. Davenport, S. Skendzic, N. Volet, J. C. Hulme, M. J. R. Heck, J. E. Bowers, *IEEE J. Select. Topics Quantum Electron.* **2016**, *22*, 78.
- [72] L. Arizmendi, *Phys. Stat. Sol. (a)* **2004**, *201*, 253.
- [73] W. Bogaerts, P. De Heyn, T. Van Vaerenbergh, K. De Vos, S. Kumar Selvaraja, T. Claes, P. Dumon, P. Bienstman, D. Van Thourhout, R. Baets, *Laser & Photon. Rev.* **2011**, *6*, 47.
- [74] A. Guarino, G. Poberaj, D. Rezzonico, R. Degl'Innocenti, P. Günter, *Nature Photonics* **2007**, *1*, 407.
- [75] J. Wang, F. Bo, S. Wan, W. Li, F. Gao, J. Li, G. Zhang, J. Xu, *Opt Express* **2015**, *23*, 23072.
- [76] A. J. Mercante, P. Yao, S. Shi, G. Schneider, J. Murakowski, D. W. Prather, *Opt Express* **2016**, *24*, 15590.
- [77] I. L. Gheorma, P. Savi, R. M. Osgood, *IEEE Photon. Technol. Lett.* **2000**, *12*, 1618.
- [78] J. A. Armstrong, N. Bloembergen, J. Ducuing, P. S. Pershan, *Physical Review* **1962**, *127*, 1918.
- [79] G. Li, Y. Chen, H. Jiang, X. Chen, *Opt Lett* **2017**, *42*, 939.
- [80] P. Mackwitz, M. Rüsing, G. Berth, A. Widhalm, K. Müller, A. Zrenner, *Appl. Phys. Lett.* **2016**, *108*, 152902.
- [81] R. V. Gainutdinov, T. R. Volk, H. H. Zhang, *Appl. Phys. Lett.* **2015**, *107*, 162903.
- [82] V. Gopalan, T. E. Mitchell, Y. Furukawa, K. Kitamura, *Appl. Phys. Lett.* **1998**, *72*, 1981.
- [83] G.-H. Shao, Y.-H. Bai, G.-X. Cui, C. Li, X.-B. Qiu, D.-Q. Geng, D. Wu, Y.-Q. Lu, *AIP Advances* **2016**, *6*, 075011.
- [84] R. Luo, H. Jiang, S. Rogers, H. Liang, Y. He, Q. Lin, *Opt Express* **2017**, *25*, 24531.
- [85] C. Wang, M. J. Burek, Z. Lin, H. A. Atikian, V. Venkataraman, I.-C. Huang, P. Stark, M. Lončar, *Opt Express* **2014**, *22*, 30924.
- [86] J. Wang, F. Bo, S. Wan, W. Li, F. Gao, J. Li, G. Zhang, J. Xu, *Opt Express* **2015**, *23*, 23072.
- [87] J. Lin, Y. Xu, Z. Fang, M. Wang, J. Song, N. Wang, L. Qiao, W. Fang, Y. Cheng, *Sci. Rep.* **2015**, *5*, 8072.
- [88] M. Wang, Y. Xu, Z. Fang, Y. Liao, P. Wang, W. Chu, L. Qiao, J. Lin, W. Fang, Y. Cheng, *Opt Express* **2017**, *25*, 124.
- [89] Z. Fang, Y. Xu, M. Wang, L. Qiao, J. Lin, W. Fang, Y. Cheng, *Sci. Rep.* **2017**, *7*, 45610.
- [90] W. C. Jiang, Q. Lin, 2016 Conference on Lasers and Electro-Optics, CLEO 2016 STu4E.6, **2016**.
- [91] W. C. Jiang, Q. Lin, *Sci. Rep.* **2016**, *1*.
- [92] T. F. Krauss, R. M. De la Rue, *Progress in Quantum Electronics* **1999**, *23*, 51.
- [93] H. Liang, R. Luo, Y. He, H. Jiang, Q. Lin, *Optica* **2017**, *4*, 1251.
- [94] L. Cai, H. Han, S. Zhang, H. Hu, K. Wang, *Opt Lett* **2014**, *39*, 2094.
- [95] S. Diziain, R. Geiss, M. Steinert, C. Schmidt, W.-K. Chang, S. Fasold, D. Fülßel, Y.-H. Chen, T. Pertsch, *Opt. Mater. Express* **2015**, *5*, 2081.
- [96] J. Hukriede, D. Runde, D. Kip, *J. Phys. D: Appl. Phys.* **2003**, *36*, R1.
- [97] L. Pierno, M. Dispenza, A. Secchi, A. Fiorello, V. Foglietti, *J. Opt. A* **2008**, *10*, 064017.
- [98] G. Ulliac, A. Lecestre, B. Guichardaz, J. Dahdah, F. I. Baida, M.-P. Bernal, N. Courjal, *Microelectronic Engineering* **2012**, *97*, 185.
- [99] M. Belt, J. Bovington, R. Moreira, J. F. Bauters, M. J. R. Heck, J. S. Barton, J. E. Bowers, D. J. Blumenthal, *Opt Express* **2013**, *21*, 1181.
- [100] E. Saitoh, Y. Kawaguchi, K. Saitoh, M. Koshiba, *IEEE Photonics J.* **2013**, *5*, 6600610.
- [101] M. A. Webster, R. M. Pafchek, A. Mitchell, T. L. Koch, *IEEE Photon. Technol. Lett.* **2007**, *19*, 429.
- [102] S. D. Siqi Duan, Y. C. Yuping Chen, G. L. Guangzhen Li, C. Z. Chuanyi Zhu, A. X. C. Xianfeng Chen, *Chin. Opt. Lett.* **2016**, *14*, 042301.
- [103] Z. Gong, R. Yin, W. Ji, J. Wang, C. Wu, X. Li, S. Zhang, *Opt Commun* **2017**, *396*, 23.
- [104] D. Dai, J. E. Bowers, *Nanophotonics* **2014**, *3*, 1.
- [105] D. Dai, J. E. Bowers, *Opt Express* **2011**, *19*, 10940.
- [106] R. C. Alferness, *Appl. Phys. Lett.* **1980**, *36*, 513.
- [107] T. Izuohara, R. Roth, R. M. Osgood, S. Bakhru, H. Bakhru, *Electron. Lett.* **2003**, *39*, 1118.
- [108] G. Schreiber, D. Hofmann, W. Grundkoetter, Y. L. Lee, H. Suche, V. Quiring, R. Ricken, W. Sohler, *Symposium on Integrated Optics* **2001**, 4277, 144.
- [109] R. Brinkmann, I. Baumann, M. Dinand, W. Sohler, H. Suche, *IEEE J. Quantum Electron.* **1994**, *30*, 2356.
- [110] C. H. Huang, L. McCaughan, *IEEE Journal of Selected Topics in Quantum Electronics* **1996**, *2*, 367.
- [111] D. L. Veasey, J. M. Gary, J. Amin, *IEEE Journal of Quantum Electronics* **1997**, *33*, 1647.
- [112] W. Sohler, *IEICE Transactions on Electronics* **2005**, *E88-C*, 990.
- [113] M. Fleuster, C. Buchal, E. Snoeks, A. Polman, *J. Appl. Phys.* **1994**, *75*, 173.
- [114] A. W. Fang, H. Park, J. E. Bowers, M. J. Paniccia, O. Cohen, R. Jones, *Opt Express* **2006**, *14*, 9203.
- [115] W. K. Chan, A. Yi-Yan, T. J. Gmitter, *IEEE Photon. Technol. Lett.* **1990**, *2*, 194.
- [116] W. K. Chan, A. Yi-Yan, T. Gmitter, L. T. Florez, *Transactions on Electron Devices* **1989**, *36*, 2627.
- [117] A. Yi-Yan, W. K. Chan, T. J. Gmitter, L. T. Florez, J. L. Jackel, E. Yablonovitch, R. Bhat, J. P. Harbison, *IEEE Photon. Technol. Lett.* **1989**, *1*, 379.

- [118] A. W. Fang, R. Jones, H. Park, O. Cohen, O. Raday, M. J. Paniccia, J. E. Bowers, *Opt Express* **2007**, *15*, 2315.
- [119] J. Brouckaert, G. Roelkens, D. Van Thourhout, R. Baets, *J. Lightwave Technol.* **2007**, *25*, 1053.
- [120] L. Shen, Y. Jiao, W. Yao, Z. Cao, J. P. van Engelen, G. Roelkens, M. K. Smit, J. J. G. M. van der Tol, *Opt Express* **2016**, *24*, 8290.
- [121] Y. Wang, Z. Wang, Q. Yu, X. Xie, T. Posavitz, M. Jacob-Mitos, A. Ramaswamy, E. J. Norberg, G. A. Fish, A. Beling, *IEEE J. Select. Topics Quantum Electron.* **2017**, *24*, 1.
- [122] M. G. Tanner, L. S. E. Alvarez, W. Jiang, R. J. Warburton, Z. H. Barber, R. H. Hadfield, *Nanotechnology* **2012**, *23*, 505201.
- [123] J. P. Höpker, M. Bartnick, E. Meyer-Scott, F. Thiele, S. Krapick, N. Montaut, M. Santandrea, H. Herrmann, S. Lengeling, R. Ricken, V. Quiring, T. Meier, A. Lita, V. Verma, T. Gerrits, S. W. Nam, C. Silberhorn, T. J. Bartley, arXiv **arXiv:1708.06232v1**, **2017**.
- [124] N. Kaneda, H. Ereifej, E. Rouvalis, J. Lee, *Ofc Th3F.4*, **2016**.
- [125] M. Y. S. Sowailam, T. M. Hoang, M. Morsy-Osman, M. Chagnon, M. Qiu, S. Paquet, C. Paquet, I. Woods, Q. Zhuge, O. Liboiron-Ladouceur, D. V. Plant, *IEEE Photon. Technol. Lett.* **2017**, *29*, 442.
- [126] J. D. Reis, *400G White Paper*. (Technology Options for 400G Implementation (OIF-Tech-Options-400G-01.0), 2015).
- [127] G. Raybon, A. Adamiecki, J. Cho, P. Winzer, A. Konczykowska, F. Jorge, J.-Y. Dupuy, M. Riet, B. Duval, K. Kim, S. Randel, D. Piloni, B. Guan, N. Fontaine, E. C. Burrows, *Ipc* **2015**, 1.
- [128] K. Takiguchi, K. Okamoto, K. Moriwaki, *IEEE Photon. Technol. Lett.* **1994**, *6*, 561.
- [129] P. Dong, C. Xie, L. L. Buhl, Y.-K. Chen, J. H. Sinsky, G. Raybon, *J. Lightwave Technol.* **2015**, *33*, 1191.
- [130] S. L. Jansen, D. van den Borne, B. Spinnler, S. Calabro, H. Suche, P. M. Kummerich, W. Sohler, G. D. Khoe, H. de Waardt, *J. Lightwave Technol.* **2006**, *24*, 54.
- [131] A. Malacarne, G. Meloni, G. Berrettini, N. Sambo, L. Poti, A. Bogoni, *J. Lightwave Technol.* **2013**, *31*, 1797.
- [132] T. Umeki, O. Tadanaga, M. Asobe, *IEEE Journal of Quantum Electronics* **2010**, *46*, 1206.
- [133] J. Yamawaku, H. Takara, T. Ohara, A. Takada, T. Morioka, O. Tadanaga, H. Miyazawa, M. Asobe, *IEEE J. Select. Topics Quantum Electron.* **2006**, *12*, 521.
- [134] H. Jiang, R. Luo, H. Liang, X. Chen, Y. Chen, Q. Lin, *Opt Lett* **2017**, *42*, 3267.
- [135] H. Kumar, V. Janyani, B. Oleh, U. Serhij, S. Dmytro, *Comsol Conference in Bangalore* **2016**.
- [136] T. Udem, R. Holzwarth, T. W. Hänsch, *Nature* **2002**, *416*, 233.
- [137] R. Holzwarth, T. Udem, T. W. Hänsch, J. C. Knight, W. J. Wadsworth, P. S. J. Russell, *Phys. Rev. Lett.* **2000**, *85*, 2264.
- [138] J. Pfeifle, V. Brasch, M. Lauerermann, Y. Yu, D. Wegner, T. Herr, K. Hartinger, P. Schindler, J. Li, D. Hillerkuss, R. Schmogrow, C. Weimann, R. Holzwarth, W. Freude, J. Leuthold, T. J. Kippenberg, C. Koos, *Nature Photonics* **2014**, *8*, 375.
- [139] P. Marin-Palomo, J. N. Kemal, M. Karpov, A. Kordts, J. Pfeifle, M. H. P. Pfeiffer, P. Trocha, S. Wolf, V. Brasch, M. H. Anderson, R. Rosenberger, K. Vijayan, W. Freude, T. J. Kippenberg, C. Koos, *Nature* **2017**, *546*, 274.
- [140] T. Hansson, F. Leo, M. Erkintalo, J. Anthony, S. Coen, I. Ricciardi, M. De Rosa, S. Wabnitz, *J Opt Soc Am B* **2016**, *33*, 1207.
- [141] Z.-J. Wu, Y. Ming, F. Xu, Y.-Q. Lu, *Opt Express* **2012**, *20*, 17192.
- [142] O. Alibart, V. D'Auria, M. D. Micheli, F. Doutre, F. Kaiser, L. Labonté, T. Lunghi, É. Picholle, S. Tanzilli, *J. Opt.* **2016**, *18*, 104001.
- [143] P. Ben Dixon, J. H. Shapiro, F. N. Wong, *Opt Express* **2013**, *21*, 5879.
- [144] J.-L. Tambasco, A. Boes, L. G. Helt, M. J. Steel, A. Mitchell, *Opt Express* **2016**, *24*, 19616.
- [145] A. Christ, A. Eckstein, P. J. Mosley, C. Silberhorn, *Opt Express* **2009**, *17*, 3441.
- [146] M. Tillmann, B. Dakić, R. Heilmann, S. Nolte, A. Szameit, P. Walther, *Nature Photonics* **2013**, *7*, 540.
- [147] G. Langrock, E. Diamanti, R. V. Roussev, Y. Yamamoto, M. M. Fejer, H. Takesue, *Opt Lett* **2005**, *30*, 1725.
- [148] R. V. Roussev, C. Langrock, J. R. Kurz, M. M. Fejer, *Opt Lett* **2004**, *29*, 1518.
- [149] C. Schuck, W. H. P. Pernice, H. X. Tang, *Appl. Phys. Lett.* **2013**, *102*, 051101.
- [150] O. Kahl, S. Ferrari, V. Kovalyuk, G. N. Goltsman, A. Korneev, W. H. P. Pernice, *Sci. Rep.* **2015**, *5*, 10941.
- [151] K. Takemoto, Y. Nambu, T. Miyazawa, Y. Sakuma, T. Yamamoto, S. Yorozu, Y. Arakawa, *Sci. Rep.* **2015**, *5*, 14383.
- [152] K. De Greve, L. Yu, P. L. McMahon, J. S. Pelc, C. M. Natarajan, N. Y. Kim, E. Abe, S. Maier, C. Schneider, M. Kamp, S. Höfling, R. H. Hadfield, A. Forchel, M. M. Fejer, Y. Yamamoto, *Nature* **2012**, *491*, 421.
- [153] C. Monroe, J. Kim, *Science* **2013**, *339*, 1164.
- [154] S. Kasture, F. Lenzini, B. Haylock, A. Boes, A. Mitchell, E. W. Streed, M. Lobino, *J. Opt.* **2016**, *18*, 1.
- [155] I. E. Zadeh, A. W. Elshaari, K. D. Jöns, A. Fognini, D. Dalacu, P. J. Poole, M. E. Reimer, V. Zwiller, *Nano Lett.* **2016**, *16*, 2289.
- [156] M. U. Staudt, S. R. Hastings-Simon, M. Nilsson, M. Afzelius, V. Scarani, R. Ricken, H. Suche, W. Sohler, W. Tittel, N. Gisin, *Phys. Rev. Lett.* **2007**, *98*, 77.
- [157] M. U. Staudt, M. Afzelius, H. de Riedmatten, S. R. Hastings-Simon, C. Simon, R. Ricken, H. Suche, W. Sohler, N. Gisin, *Phys. Rev. Lett.* **2007**, *99*, 77.
- [158] N. Sinclair, E. Saglamyurek, M. George, R. Ricken, C. La Mela, W. Sohler, W. Tittel, *Journal of Luminescence* **2010**, *130*, 1586.
- [159] N. Sinclair, E. Saglamyurek, H. Mallahzadeh, J. A. Slater, M. George, R. Ricken, M. P. Hedges, D. Oblak, C. Simon, W. Sohler, W. Tittel, *Phys. Rev. Lett.* **2014**, *113*, 053603.
- [160] J. Bennès, S. Ballandras, F. Chérioux, *Applied Surface Science* **2008**, *255*, 1796.
- [161] K. Länge, B. E. Rapp, M. Rapp, *Anal Bioanal Chem* **2008**, *391*, 1509.
- [162] K. K. Mehta, G. N. West, R. J. Ram, *Cleo* **2017**, **2017**, 1.
- [163] M. C. Estevez, M. Alvarez, L. M. Lechuga, *Laser & Photon. Rev.* **2011**, *6*, 463.
- [164] D. Richter, P. Weibring, A. Fried, O. Tadanaga, Y. Nishida, M. Asobe, H. Suzuki, *Opt Express* **2007**, *15*, 564.